Description of the Response of Materials to Pulsed Thermonuclear Radiation - Part II

T.O. Hunter and G.L. Kulcinski

September 1977

UWFDM-217

FUSION TECHNOLOGY INSTITUTE

UNIVERSITY OF WISCONSIN

MADISON WISCONSIN

Description of the Response of Materials to Pulsed Thermonuclear Radiation - Part II

T.O. Hunter and G.L. Kulcinski

Fusion Technology Institute
University of Wisconsin
1500 Engineering Drive
Madison, WI 53706

http://fti.neep.wisc.edu

September 1977

UWFDM-217

Description of the Response of Materials to Pulsed Thermonuclear Radiation

(Part II)

Transient Energy Deposition, Temperatures, and Displacement Rates

Thomas O. Hunter*
G.L. Kulcinski

UWFDM-217

October 1977

*Member Technical Staff, Sandia Laboratories, Albuquerque, New Mexico, 87115
Work partially supported by Energy Research & Development Administration

Fusion Research Program
University of Wisconsin
Madison, Wisconsin 53706

ABSTRACT

General response models are developed for materials exposed to transient thermonuclear radiation. Models and data are discussed for determining the energy deposition for photons, low Z ions, high Z ions, and neutrons. Temperature response solutions commensurate with the deposition models are developed. A thermoelastic wave solution which can be applied to arbitrary radiation spectra is discussed. A general technique for determining the nuclear displacement damage for ion radiation is developed.

The result of the application of these models in the computer code T-DAMEN is displayed for copper exposed to a reference laser fusion spectrum.

Table of Contents

I. Introduction

Part I[1] of this document outlined a systematic investigation of the effects of transient thermonuclear radiation on materials which are used in reactor first walls, liners and other components.

This section (Part II) contains more specific information on the transient deposition, temperature, displacement rate and stress responses. General models are developed to accommodate most spectra which may be encountered in inertial confinement fusion systems. These models in many cases incorporate the initial developments given in Part I and extend them to more general cases.

The objectives of Part II are to specify the data and analytical techniques which can be used for transient material response and to apply these models to materials irradiated with representative spectra. The models presented are not specific to any design concept as characterized by a fuel type, wall loading, material, or cavity radius. They are, however, subject to some limitations. The depositions of photons are considered as exponential in space without considering subsequent transport. The slowing down calculations are based on techniques which do not consider the effect of the free surface in the ion interaction process.

The temperature response is limited to materials which maintain a single phase; that is, the coupled hydrodynamics and thermodynamics of ablation and melting are not considered. The superposition of the responses to several radiation types requires linearity in all temperature models.

The portion of the transient irradiation phenomenology outlined in Part I which is addressed in Part II is shown in Figure 1. Future documents will provide more information on other phenomena.

Chapter II contains the models developed for this study and includes illustrative examples of the interaction processes and responses for a reference material. Chapter III consists of the results of the application of the models to the irradiation of a selected material by a characteristic spectrum which consists of various radiation components.

Figure 1

TRANSIENT IRRADIATION PHENOMENOLOGY

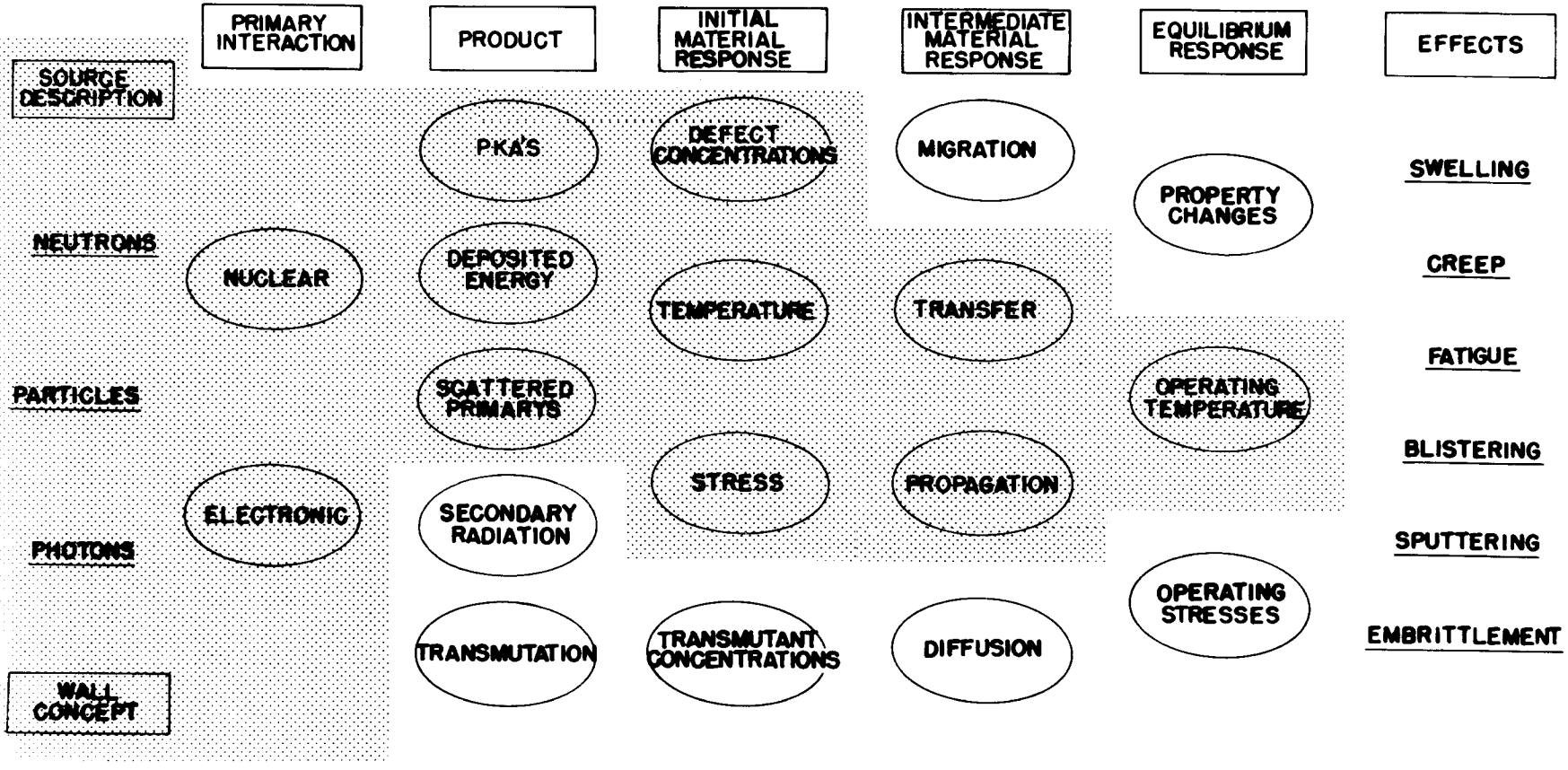

COVERED IN THIS DOCUMENT

II. Response Models

The deposition, temperature and displacement response of a material are functions of the flux, energy and type of the irradiating species. It is convenient for determining the respective phenomena to segregate the species into four categories:

a) photons

b) ions ($Z \leq 2$)

c) ions ($Z \geq 2$)

d) neutrons

The associated response for each category is presented in the following sections.

II-A. Energy Deposition

II-A-1. Photons

The energy deposition of laser light and X-rays is covered in detail in Part I. The X-ray data is based on the work of Biggs[2] and has been incorporated into this study by developing a general library of photoelectric cross sections for all elements ($1 < Z \leq 100$), which can be accessed by specification of the atomic number of a material and photon energy considered. Incoherent cross sections are derived from the representation of the Klien-Nishina formula developed by Biggs. The cross sections determine the

absorption profiles which are considered pure exponentials in space. For high energy photons (>30 kev for carbon) the photoelectric cross sections are negligible compared to those associated with incoherent scattering. For these spectra the total incoherent cross sections are used in this study. This assumption will always overestimate the primary energy near the surface since scattering and transport are not assumed. The fact that the energy deposition may be overestimated near the exposed surface of a material means it may be underestimated further into the material. However, this approximation is considered reasonable for most applications since the average scattered photon energy is significantly lower than the incident photon energy and, as a result, is shifted towards the region where it will be more readily absorbed by the photoelectric process. Examples of the sum of the photoelectric and incoherent total cross section for C, Cu, Mo, and Ta are shown in Figure 2.

Laser light absorption, especially for high intensity beams, has limited coverage in the open literature; hence the simple models discussed in Part I are retained here.

II-A-2. Ions ($Z \leq 2$)

Energetic light ions which are present in inertial confinement fusion systems, e.g., He, D, T, lose kinetic energy in materials primarily by electronic interaction when their energy is above a few keV. Consequently,

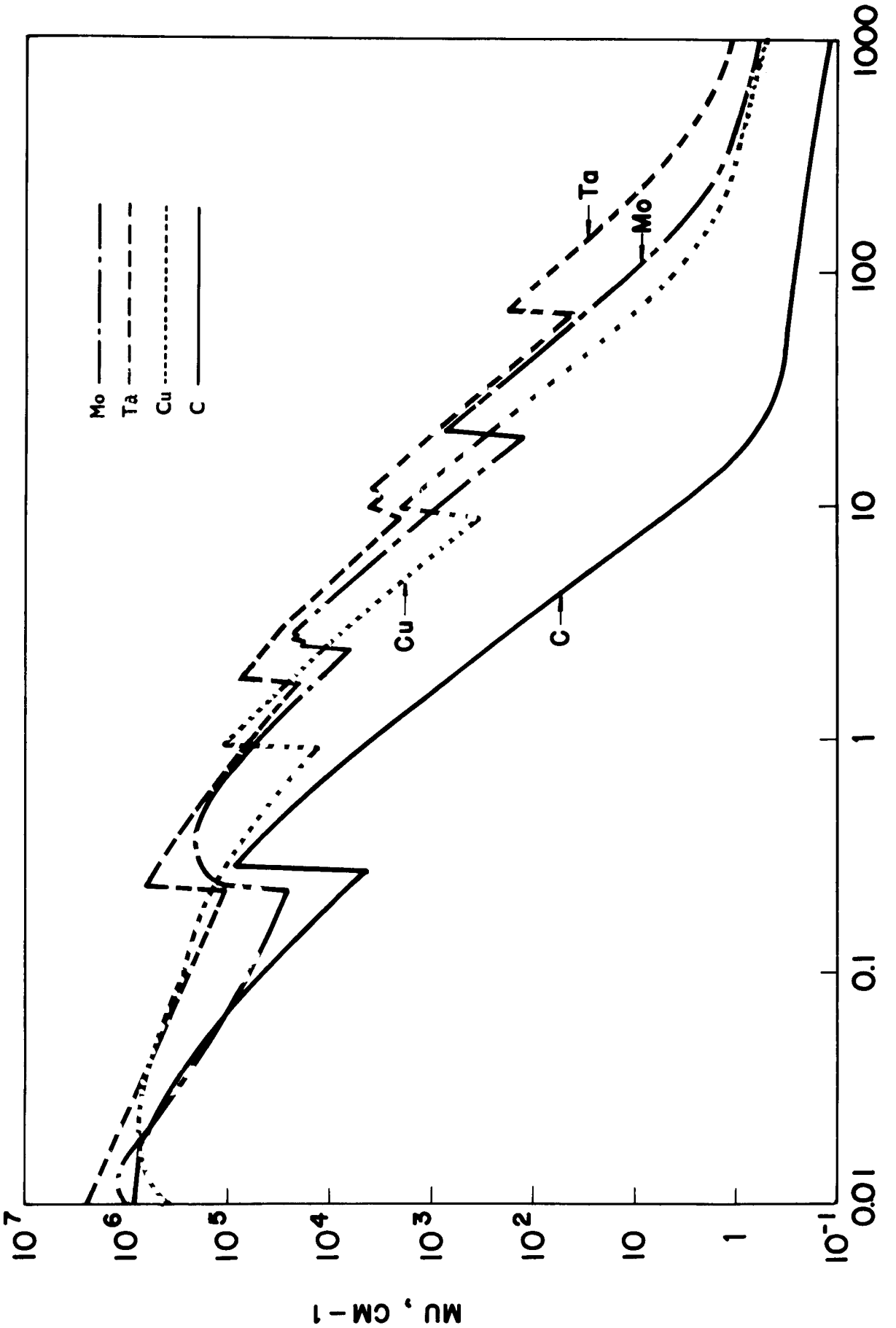
TOTAL PHOTON CROSS SECTION
Mo
Ta
Cu
C
Ta
Mo
Cu
C
MU , CM - 1
ENERGY, KEV
10^7
10^6
10^5
10^4
10^3
10^2
10
1
10^-1
0.01
0.1
1
10
100
1000

Figure 2

the transport equation which governs their spatial distribution is dominated by the ionization or "frictional" term. This feature was illustrated in Part I where a comparison of the nuclear and electronic loss terms for He in carbon was made. This domination by electronic processes allows the spatial distribution to be determined upon knowledge of the stopping power for the ion in a material.

The spectra from thermonuclear microexplosions consist of ions whose energies fall in all three regions of energy loss:

Region I - the low energy region where the incoming ion has lost its original charge state where energy loss increases with energy.

Region II - the intermediate region where the charge state can vary from zero to a finite value less than the total ionization state and energy loss reaches a maximum.

Region III - the high energy region where total ionization is achieved and energy loss decreases with increasing energy.*

In Part I it was shown that neither the Bethe-Bloch[3] or Lindhard[4] (LSS) models are entirely adequate in all of the regions. The Brice[5] formulation, however, since it is semi-empirical, can reproduce the experimental data with reasonable accuracy. This study has, therefore, relied on the Brice fomulation for electron energy loss data. The defining equations for this model are Equations 24, 25, and 26 in Part I.

---

* for non relativistic particles.

These equations will reproduce the stopping power data as a function of energy. The desired result for response studies is energy deposited as a function of distance. Hence, a transformation must be made to determine the mean location of an ion. The Brice formulae cannot be easily transformed to yield a closed form expression for the mean spatial distribution and, hence, difference codes are normally used which integrate the transport equations numerically.

This study required analytic forms for the spatial distribution which could be readily evaluated and which yielded accuracy comparable to the data available. As a result the deposition and local mean ion energy were determined in terms of a standard set of functions of space.

The stopping power data (as reproduced by the Brice formula) were divided into three regions roughly corresponding to those mentioned above as shown in Figure 3. In each region a function was found which would reproduce the data and which could be transformed into spatial functions which are in a closed form.

The following functions were found:

1) $\frac{dE}{dx}(E) = - S_o \, (E/E_o)^{1/2}$ Region 1

2) $\frac{dE}{dx}(E) = - A_1 \, (1 - e^{-B_1 E})$

or, 3) $\frac{dE}{dx}(E) = - [D^2 - P^2 (E - B_2)^2]$ } Region 2

4) $\frac{dE}{dx}(E) = - A_3 \, e^{-E/B_3}$ Region 3

Figure 3

GENERAL ELECTRONIC ENERGY LOSS FUNCTION

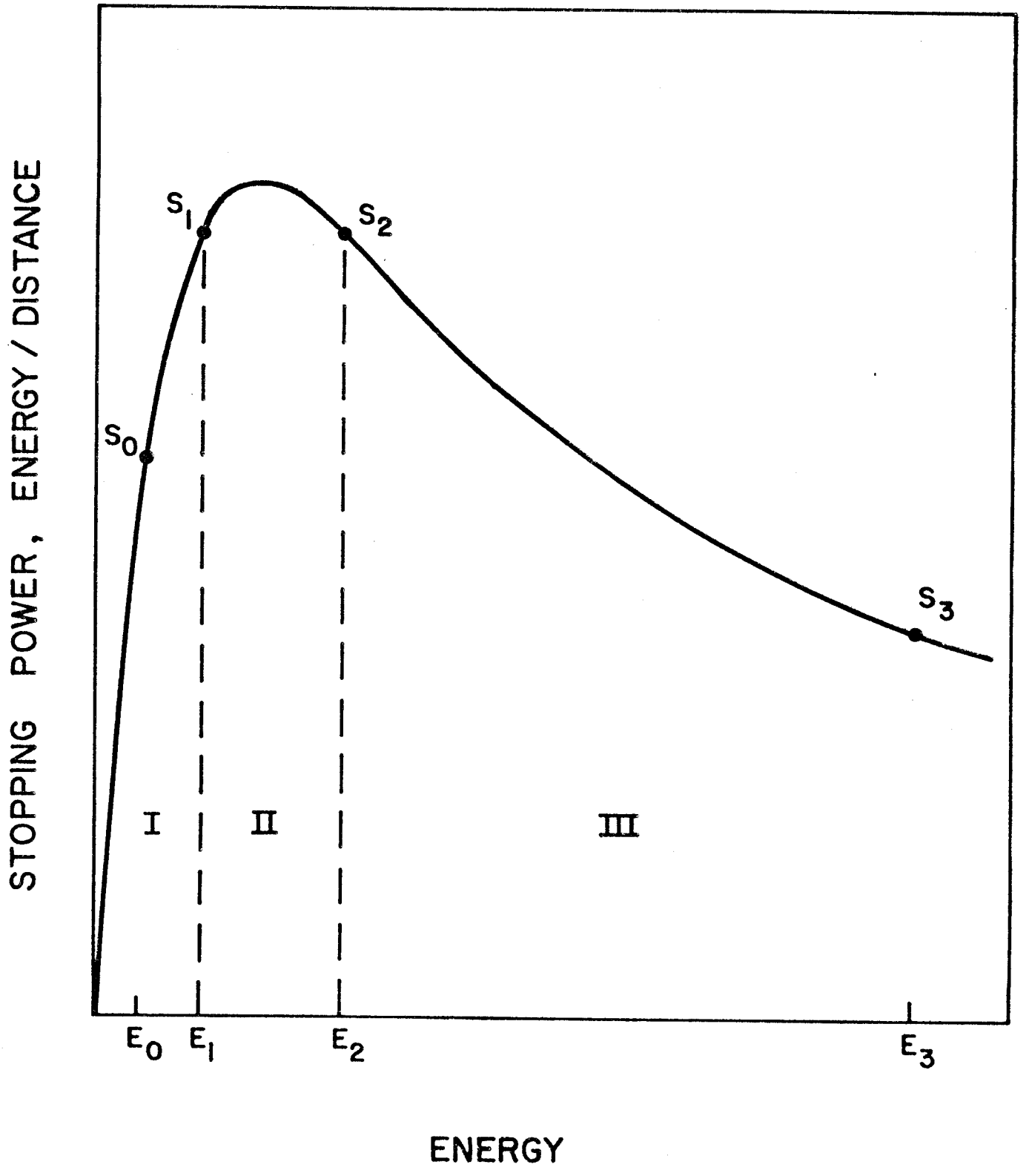

where S_o, E_o, A_1, B_1, D, P, B_2, A_3, B_3 are all constants.

These equations were chosen because they can be readily transformed by the process:

$$5) \quad X(E) = \int_{E^*}^{E} \frac{1}{dE/dx(E)}\, dE$$

where E* is the incident ion energy.
Equation 5 can then be solved for E, such as,

$$6) \quad E = F(x,E^*)$$

and

$$7) \quad \frac{dE}{dx}(x) = \frac{dE}{dx}(F(x,E^*)) \text{ or } = \frac{d}{dx} F(x,E^*) \ .$$

The results of performing these transformations for each of the equations yields the spatial distributions and local energy fractions given in Table I.

The constants for each region can be determined by selecting reference points, as illustrated in Figure 3, from the stopping power curve and using the relation shown in Table II.

Upon determination of the constants in Equations 1-4, the depositions are completely determined as functions of space. The deposition functions will be continuous in space, but the curvature of each function will be discontinuous where the regions I, II, and III are joined.

Table I

	Equation Number	Spatial Distribution	Local Energy
Region 1	1	$\frac{dE}{dx}(x) = S_o \left(\frac{E^*}{E_o}\right)^{1/2} - \frac{S_o^2 x}{2E_o}$	$E(x) = E^* - S_o x \left(\frac{E^*}{E_o}\right)^{1/2} + \frac{S_o^2 x^2}{4E_o}$
	2	$\frac{dE}{dx}(x) = \frac{A_1}{e^{B_1(A_1 x - Q_1)} + 1}$ $Q_1 = E^* + \frac{\ell n}{B_1}(1 - e^{-B_1 E^*})$	$E(x) = \frac{1}{B_1} \ell n \left(1 + e^{+B_1(Q_1 - A_1 x)}\right)$
Region 2	3	$\frac{dE}{dx}(x) = \frac{D^2 4z}{(1+z)2}$ $z = e^{(Q_2 - x)2D\sqrt{p}}$	$E(x) = \frac{D}{p} \frac{(z-1)}{(z+1)} + B_2$ $Q_2 = \frac{1}{2Dp} \ell n \left(\frac{D/p + E^* - B_2}{D/p - E^* + B_2}\right)$
Region 3	4	$\frac{dE}{dx}(x) = \frac{A_3 e^{-E^*/B_3}}{1 - \frac{A_3 x}{B_3} e^{-e^*/B_3}}$	$E(x) = B_3 \ell n \left[e^{E^*/B_3} - A_3 x / B_3\right]$

In all cases x is measured from the point where $E = E^*$

Table II

Evaluation of Constants

Equation	
1	S_o, E_o read directly from curve
2	$A_1 = \frac{S_o^2}{2S_o - S_1}$ $\quad B_1 = -\ \ln\ (1 - S_o/A_1)$
	where E_o, S_o; E_1, S_1 are given and $E_1 = 2\ E_o$
3	$D^2 = S_{max}$ $\quad B_2 = (E_1+E_2)/2$ $\quad P = (S_{max} - S_2)/(E_2 - B_2)^2$
4	$B_3 = (E_3 - E_2)/\ \ln(S_2/S_3)$ $\quad A_3 = S_2\ e^{E_2/B_3}$

Equations 1-4, although useful in specifying the depositions, are not necessarily in a form which can be utilized by a response model; consequently, a standard form was chosen for expressing the general deposition function. The form chosen was a general polynomial represented by

$$8) \quad D(x) = A_1 + A_2x + A_3x^2 + A_4x^3 + A_5x^4 \ , \ x_a < x < x_b \ .$$

This form can be derived from the relations 1-4 if the spatial domain is divided into three regions (Figure 4) which correspond to the energy regions shown in Figure 3. The values are chosen so that the following correspondence is maintained:

Location	Energy
x_L	0
x_H	E_1
x_M	E_2
0	E^*

where E^* is the incident energy of the ion. If E^* is less than E_2 but greater than E_1, the value for x_m simply vanishes and the point $x = 0$ is simply within region II.

Figure 4

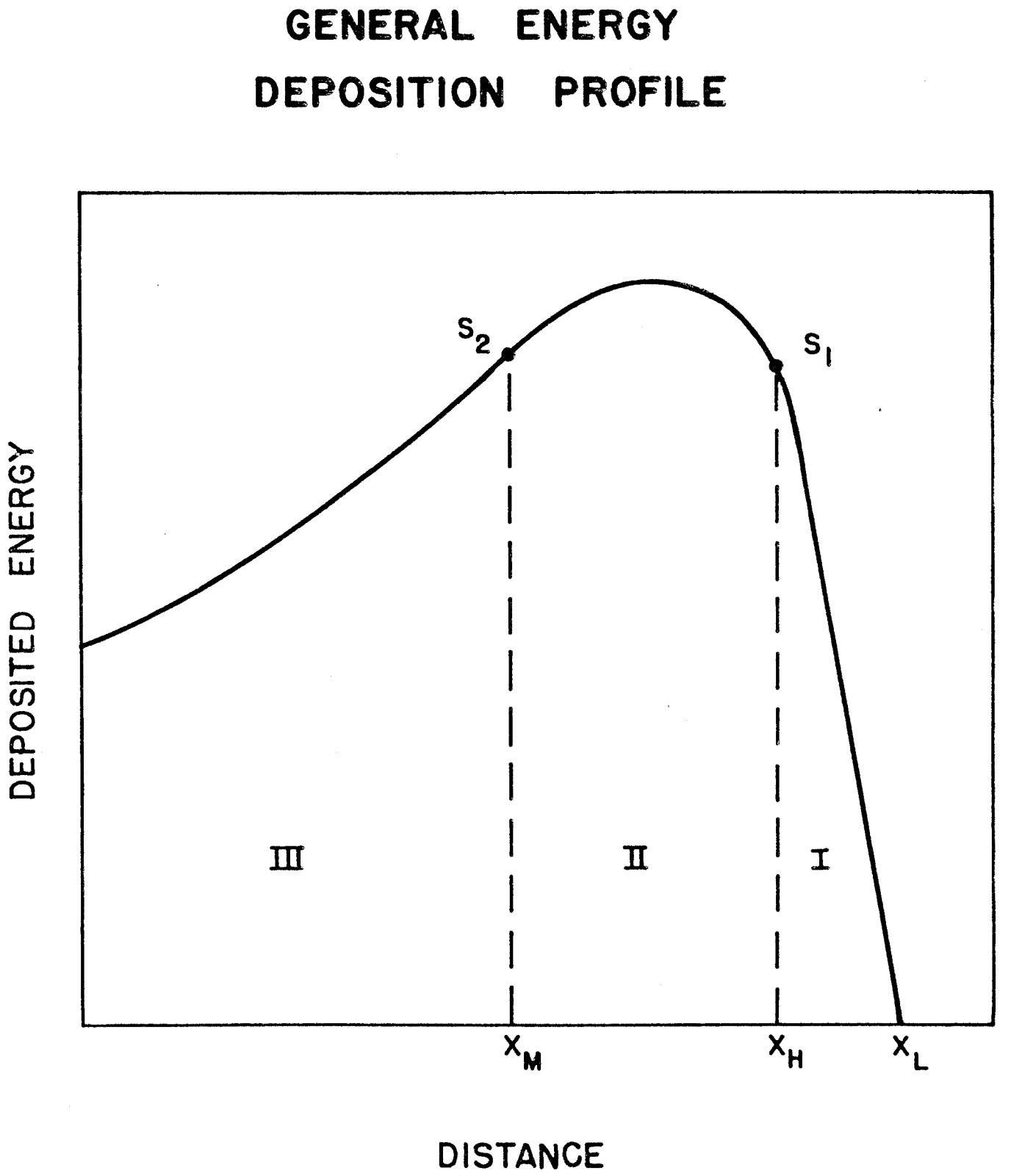
GENERAL ENERGY
DEPOSITION PROFILE
DEPOSITED ENERGY
S_2
S_1
III
II
I
X_M
X_H
X_L
DISTANCE

A similar modification is made for ions with energies less than E_1 where x_H and x_M vanish and the entire distribution is within region I.

Within each region a relation similar to Equation 6 can be derived and the coefficients determined. The result is a general expression

$$
\begin{aligned}
&D(x) = 0 \qquad x_L < x \\
&D(x) = \sum_{N=1}^{5} A_{1N}\, x^{N-1}, \quad x_H < x < x_L \\
&D(x) = \sum_{N=1}^{5} A_{2N}\, x^{N-1}, \quad x_m < x < x_H \\
&D(x) = \sum_{N=1}^{5} A_{3N}\, x^{N-1}, \quad 0 < x < x_m \ .
\end{aligned}
\tag{9}
$$

A set of relations (eq. 9) can be derived for each incident ion energy and is then available for subsequent use for any response which needs an analytic expression for the deposition.

The deposition function for region III (Equation 4) can easily be transformed into the form given in Equation 9 since it is of the form

$$y = \frac{c}{1-Bx} \tag{10}$$

which for small values of x can be expanded as

$$y = c\,(1 + Bx + (Bx)^2 + (Bx)^3 + \ldots)\ ;$$

hence the relations become

$$A_{31} = A_3 e^{-E^*/B_3}$$

$$A_{32} = A_{31}^2/B_3$$

11) $$A_{33} = A_{31}^3/B_3^2$$

$$A_{34} = A_{31}^4/B_3^3$$

$$A_{35} = A_{31}^5/B_3^4$$

For Equations 2 and 3 no simple expansion is available. In this case the coefficients can be found by evaluating a few points (e.g. n points) directly from the equations and fitting these points with an interpolatory polynomial (of order n-1).

It should be noted that Equation 1 is already in the form of Equation 9 so that:

$$A_{11} = S_o \left(\frac{E^*}{E_o}\right)^{1/2}$$

12) $$A_{12} = - S_o^2/2\ E_o$$

$$A_{13} = A_{14} = A_{15} = 0 \ .$$

Examples of the accuracy of this technique are given in Figures 5, 6, 7 in which deposition functions are depicted for helium ions into nickel for energy ranges from 200 keV to 4 MeV. Figure 5 gives the stopping power for the Brice electronic energy loss formulation (solid line) with a comparison of the function of equations (1-4) (dotted line). Fig. 6 shows the spatial deposition functions as generated from this work corresponding to various incident energies. Also in Figure 6 are deposition values determined by the more formal ion implantation computer codes by Brice.[6] The agreement by the simple calculation developed in this study is notable. Figure 7 gives the mean local ion energy (calculated from equation 1-12) as a function of space for the various incident energies.

II-A-3. Ion Deposition ($Z > 2$)

For heavy ions the energy deposition is more complex since it is no longer possible to exclude the nuclear energy loss from consideration. Consequently the general transport equation must be solved taking into account the energy dependent nuclear interaction cross sections which are also anisotropic. Various approximate solutions are available for such calculations. Three of the most widely used methods are those of Brice[6], Winterbon[7] and Manning and Mueller[8].

In general these methods develop the moments about the origin of the nuclear energy loss (damage), electronic energy loss (ionization) and particle distribution (range). These moments can then be used to reconstruct the distribution. A complete solution for this distribution is contained in the computer codes RASE4 and DAMG2[9]. These codes represent a compromise between the relatively simple EDEP 1 code of Manning and Mueller[8] and the more complex method of Winterbon.[7]

Figure 5

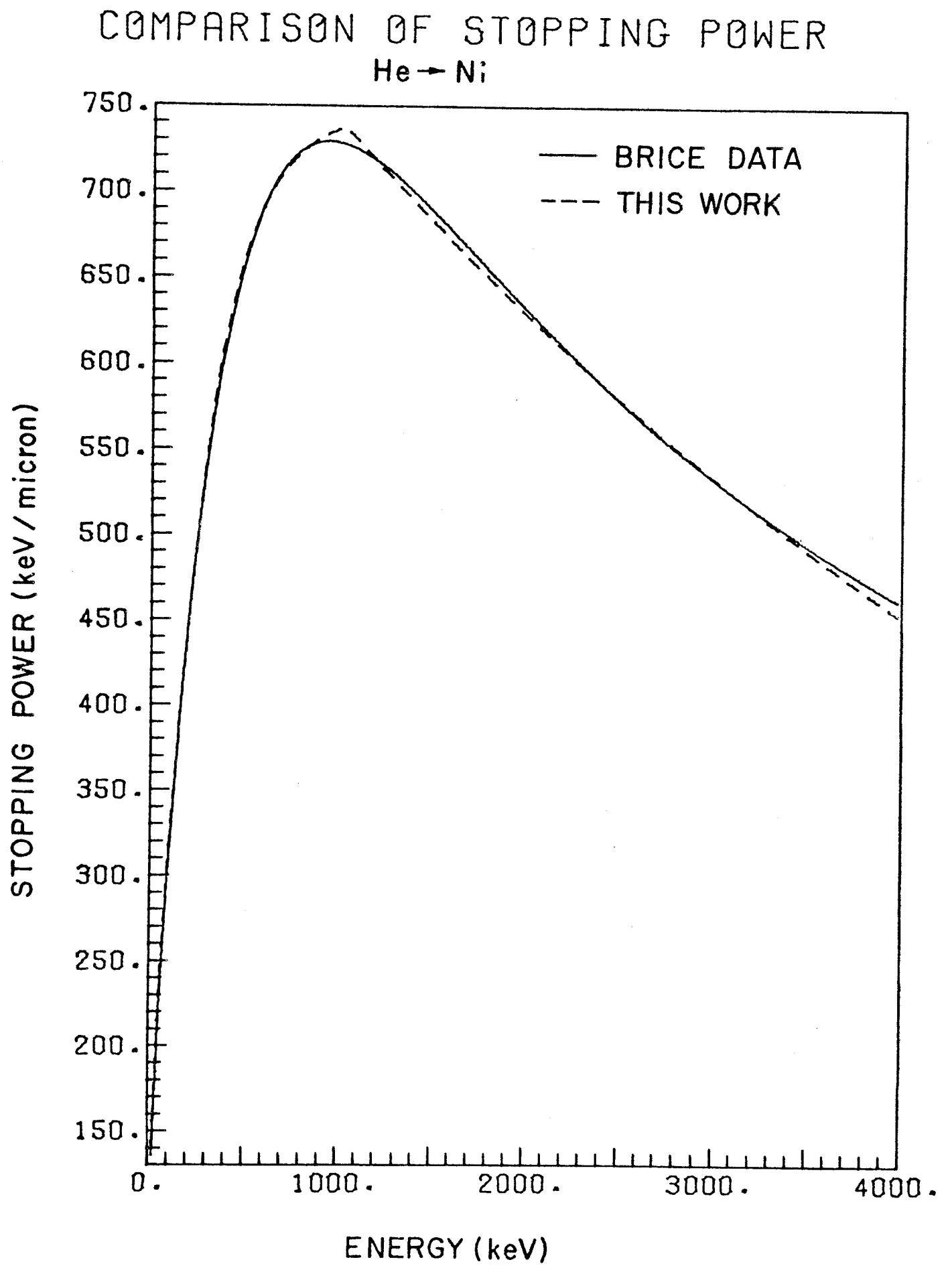
COMPARISON OF STOPPING POWER
He → Ni
BRICE DATA
THIS WORK
STOPPING POWER (keV/micron)
ENERGY (keV)
750.
700.
650.
600.
550.
500.
450.
400.
350.
300.
250.
200.
150.
0.
1000.
2000.
3000.
4000.

Figure 6

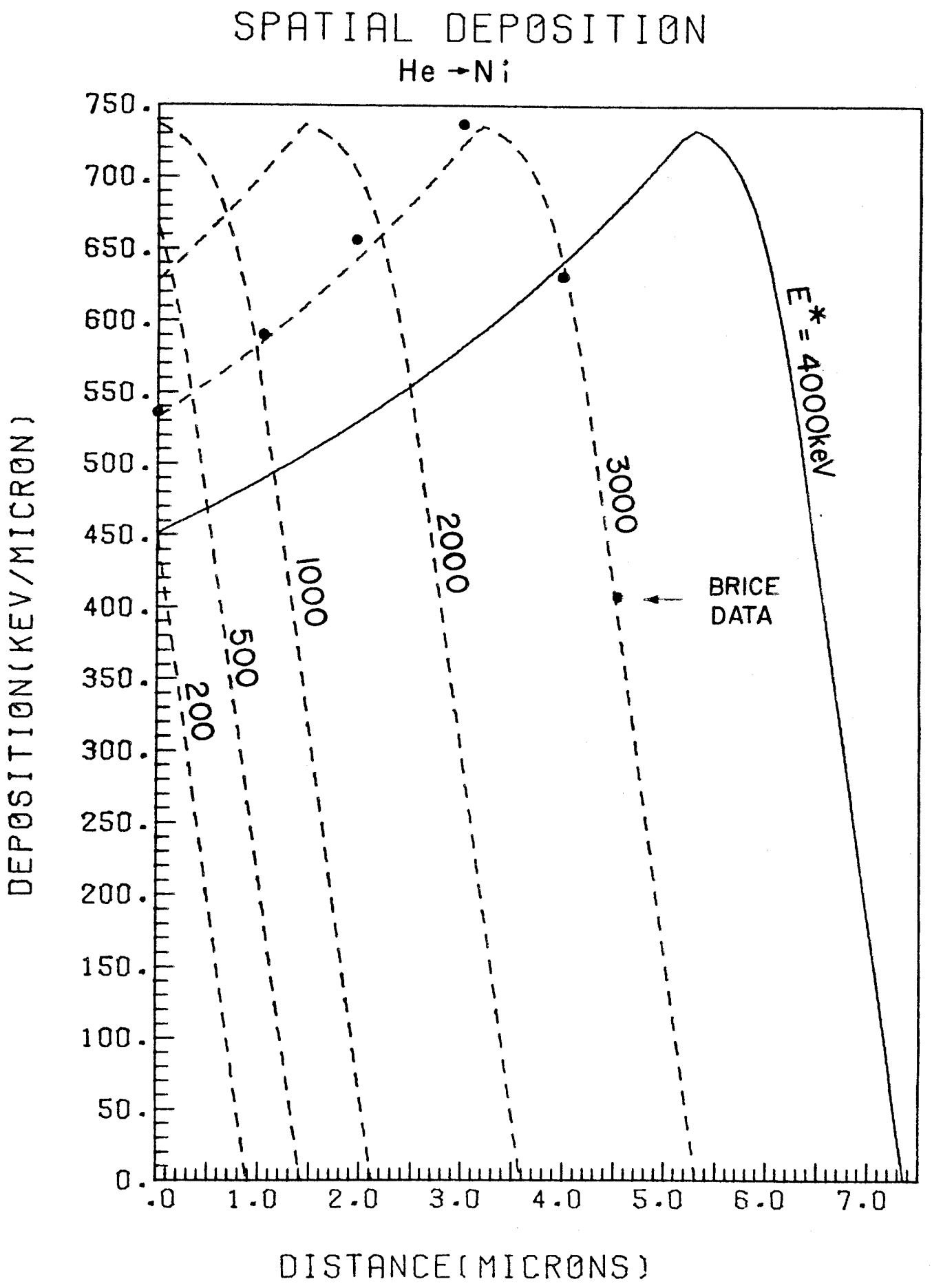
SPATIAL DEPOSITION
He → Ni
DEPOSITION(KEV/MICRON)
DISTANCE(MICRONS)
750.
700.
650.
600.
550.
500.
450.
400.
350.
300.
250.
200.
150.
100.
50.
0.
.0
1.0
2.0
3.0
4.0
5.0
6.0
7.0
200
500
1000
2000
3000
E* = 4000keV
BRICE
DATA

Figure 7

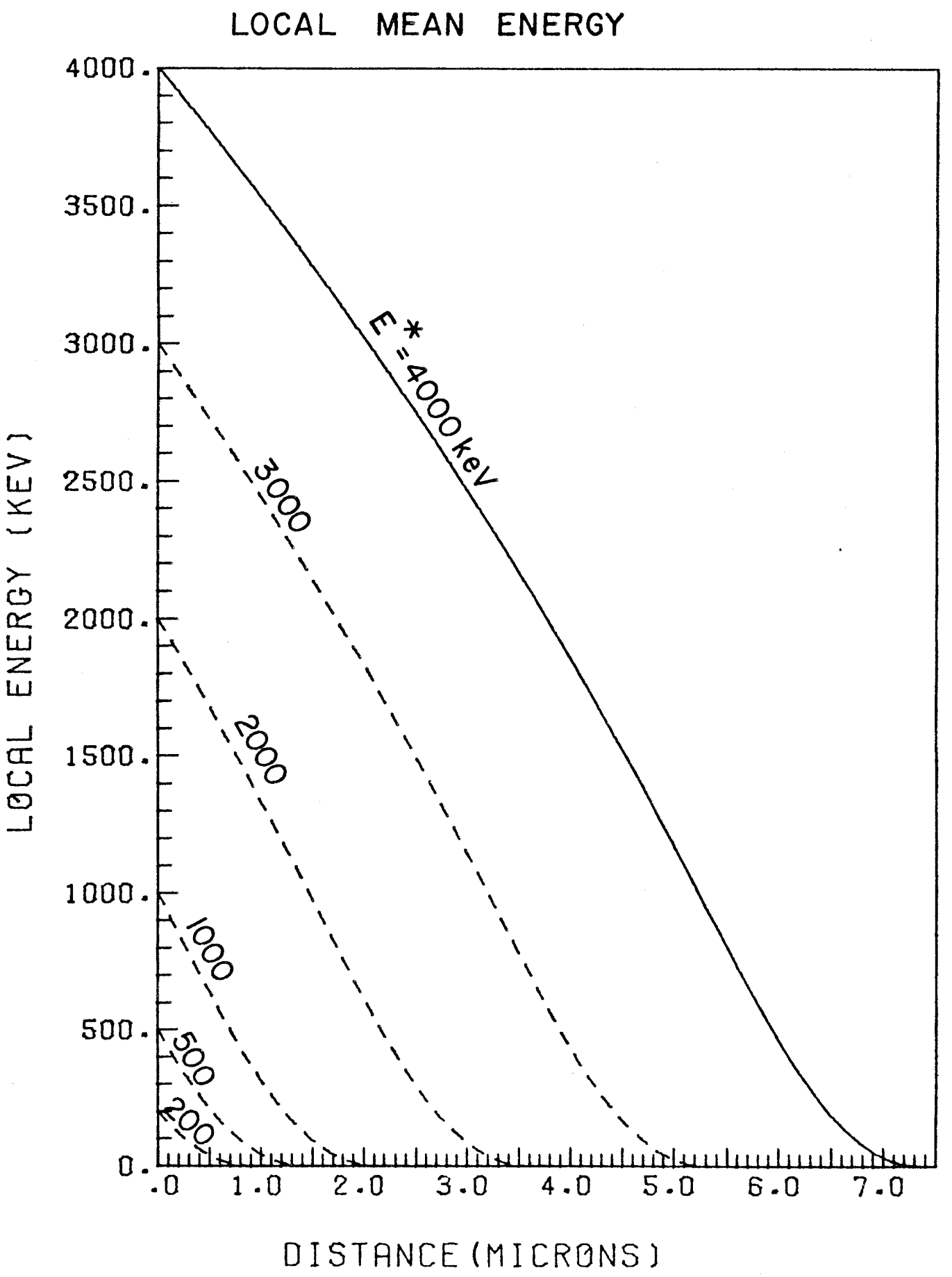
LOCAL MEAN ENERGY
4000.
3500.
3000.
2500.
2000.
1500.
1000.
500.
0.
LOCAL ENERGY (KEV)
E*=4000 keV
3000
2000
1000
500
200
.0
1.0
2.0
3.0
4.0
5.0
6.0
7.0
DISTANCE (MICRONS)

In this study an examination of the results of the RASE4 and DAMG2 codes was made to develop a general method of reproducing the results for use in a response calculation. An example of the code calculation for the deposition of aluminum ions into nickel is given in figures 8, 9, and 10. The nuclear damage is shown in figure 8 for 5 incident ion energies. It can be seen that the peak damage values occur when the interaction cross section reaches a maximum and there is a depression of damage near the surface which is due to the anisotropic redistribution of damage energy by the primary knock-on atoms (PKA). The electronic energy loss is shown in figure 9 and shows a maximum value at the surface with a decreasing function thereafter. This result is consistent with ion target combinations in which the stopping power is primarily contained in region 1 discussed previously and encompasses virtually all heavy ions of interest in fusion systems.* The sum of the nuclear and electronic contributions is shown in figure 10 and indicates that even for this combination the dominant factor is the electronic loss. This relationship is expected to occur in any model which is based on the LSS theory. A comparison of the relative amplitudes of nuclear and electronic energy loss can be seen in figure 11 which indicates that for reduced energies, ε, of 3 or more the electronic energy loss is larger. The value of k (discussed in Part I) ranges from $2 \rightarrow .1$. Hence, a more practical criterion for assurance of ionization dominance would be to select a reduced energy value of 5. Table III indicates the electronic factor, k, and the reduced energy in keV for various ion target combinations.

---

*This must be modified in the case of an extremely heavy projectile and a low Z target.

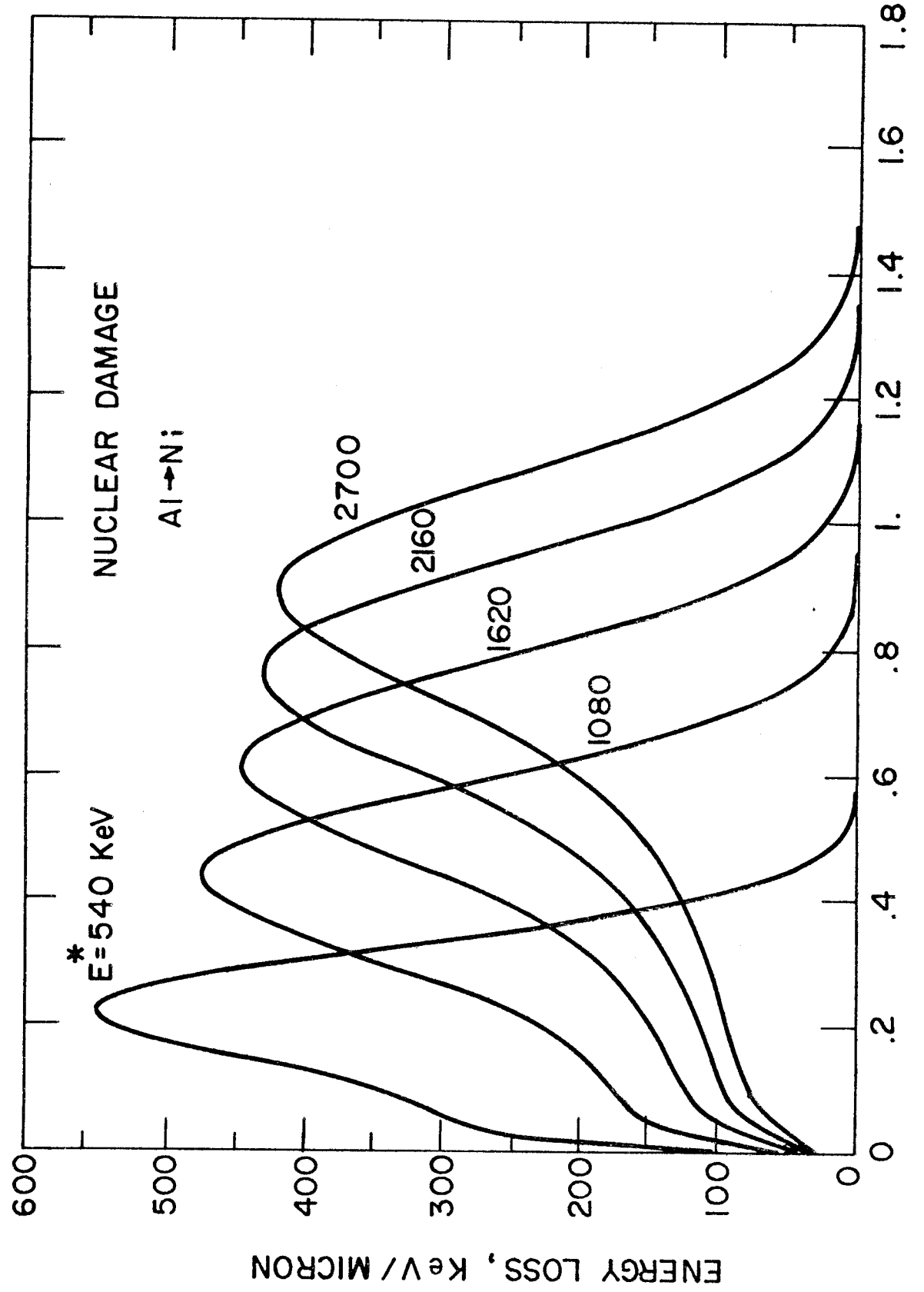
NUCLEAR DAMAGE
Al→Ni
*E=540 KeV
2700
2160
1620
1080
ENERGY LOSS, KeV/MICRON
LOCATION, MICRON
600
500
400
300
200
100
0
.2
.4
.6
.8
1.
1.2
1.4
1.6
1.8

Figure 8

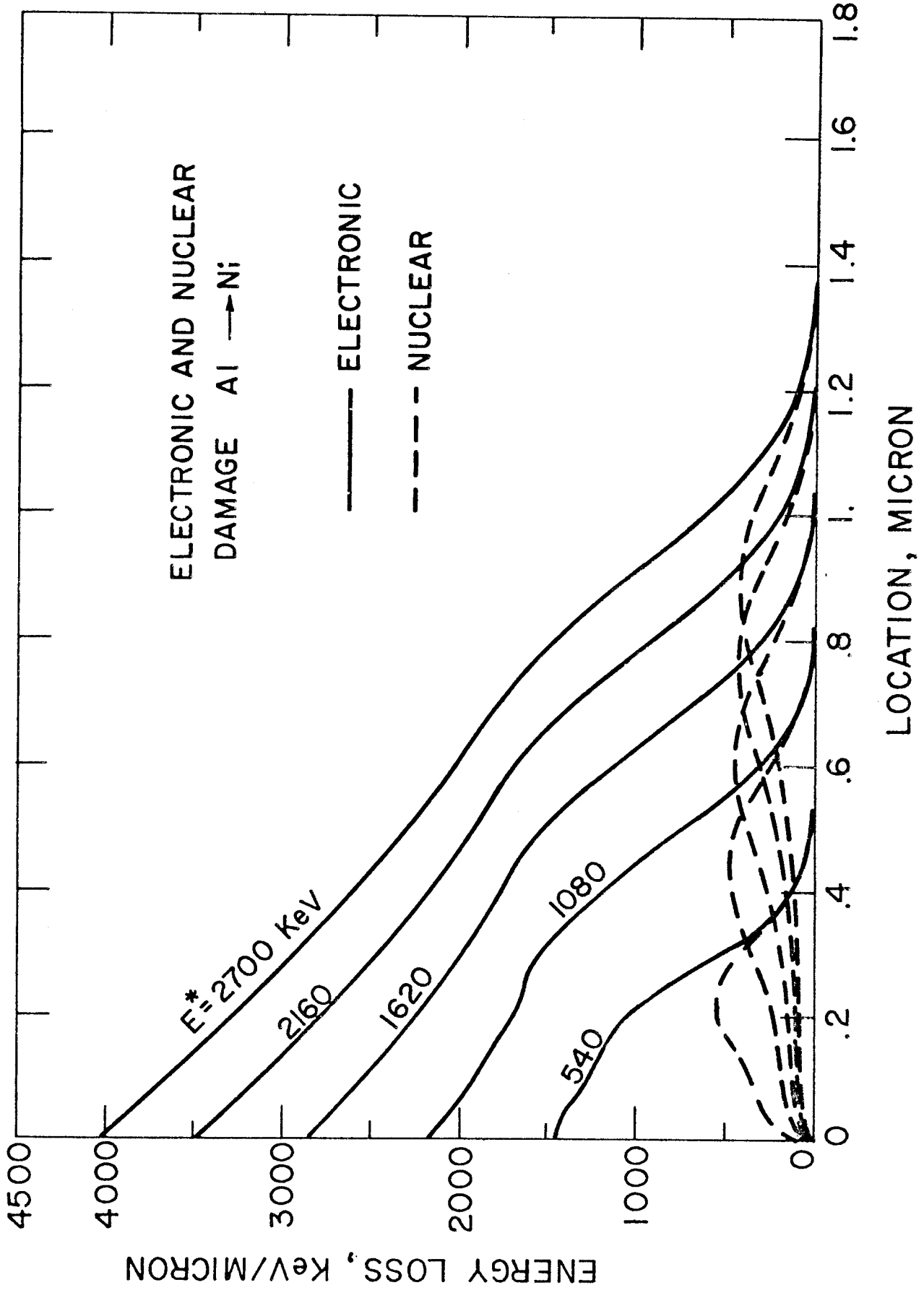
ELECTRONIC AND NUCLEAR
DAMAGE Al → Ni
ELECTRONIC
NUCLEAR
E*=2700 KeV
2160
1620
1080
540
ENERGY LOSS, KeV/MICRON
LOCATION, MICRON
4500
4000
3000
2000
1000
0
.2
.4
.6
.8
1.
1.2
1.4
1.6
1.8

Figure 9

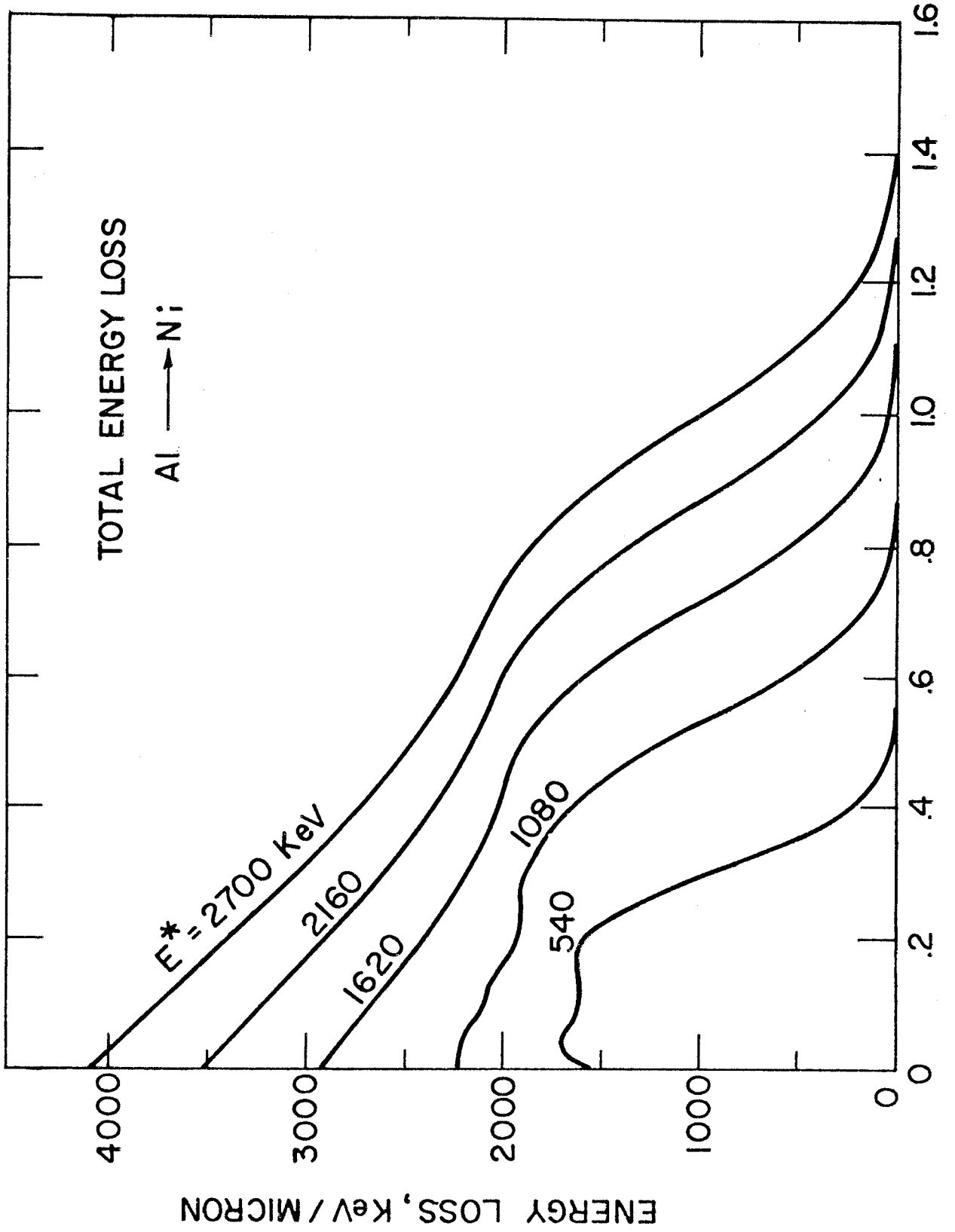
TOTAL ENERGY LOSS
Al → Ni
E* = 2700 KeV
2160
1620
1080
540
ENERGY LOSS, KeV / MICRON
LOCATION, MICRON
4000
3000
2000
1000
0
.2
.4
.6
.8
1.0
1.2
1.4
1.6

Figure 10

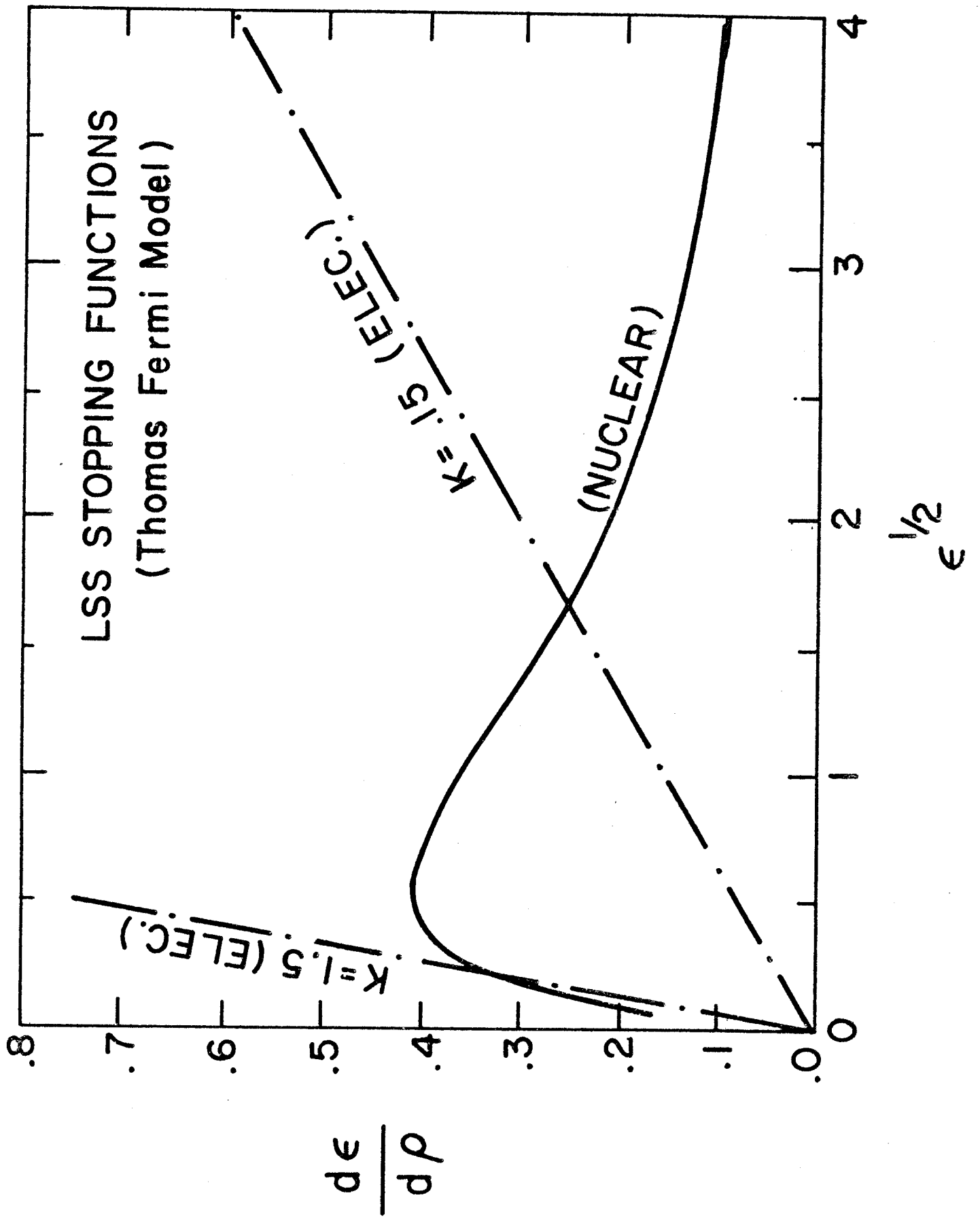
LSS STOPPING FUNCTIONS
(Thomas Fermi Model)
K=1.5 (ELEC.)
K=1.15 (ELEC.)
(NUCLEAR)
dε/dρ
ε^1/2
0
1
2
3
4
.1
.2
.3
.4
.5
.6
.7
.8

Figure 11

TABLE III

LINDHARD PARAMETERS

$\left\{\frac{k}{E_L(KEV)}\right\}$

Ion \ Target	C	Al	Ni	Mo	Ta	U
C	$\frac{.127}{5.7}$	$\frac{.208}{10.3}$	$\frac{.388}{22.0}$	$\frac{.601}{34.2}$	$\frac{1.10}{65.4}$	$\frac{1.44}{86.8}$
Al	$\frac{.105}{23.2}$	$\frac{.142}{34.6}$	$\frac{.228}{62.8}$	$\frac{.328}{90.3}$	$\frac{.567}{161.}$	$\frac{.730}{208.}$
Ni	$\frac{.103}{108.}$	$\frac{.119}{136.}$	$\frac{.161}{207.}$	$\frac{.209}{269.}$	$\frac{.326}{430.}$	$\frac{.407}{537.}$
Mo	$\frac{.104}{273.}$	$\frac{.112}{320.}$	$\frac{.137}{440.}$	$\frac{.165}{533.}$	$\frac{.236}{784.}$	$\frac{.285}{950.}$
Ta	$\frac{.111}{987.}$	$\frac{.113}{1080.}$	$\frac{.124}{1330.}$	$\frac{.137}{1480.}$	$\frac{.173}{1940.}$	$\frac{.199}{2240.}$
U	$\frac{.115}{1720.}$	$\frac{.115}{1840.}$	$\frac{.122}{2180.}$	$\frac{.131}{2360.}$	$\frac{.157}{2940.}$	$\frac{.176}{3320.}$

II-A-4. Neutron Depositions

The deposition of energy from neutrons in inertial confinement fusion is evaluated by first determining the local flux in the exposed material (both the source and scattered contributions) and then multiplying by the Kerma factor for each neutron group. This method was outlined in Part I. It is important to note however, that the volumetric energy deposition is small ($\sim$1J/cm^3 for 10^{13} N/cm^2 exposure) and hence the temperature transients are small. The deposition is typically uniformly distributed in space and initial gradients are small.

II-B. Temperature Response

The temperature response of a material exposed to thermonuclear radiation may be determined upon specification of the time and space dependent energy deposition. In this section several analytical models are given which can be used for determining the temperature at arbitrary locations and times for photon and various ion depositions.

II-B-1. Photon Models

Since photon models assume exponential spatial profiles, it is only necessary to state the boundary conditions for an exposed material to formulate a model. In part I, a general solution for a finite width, one dimensional slab was given for both single and multiple pulses of photon irradiation. For completeness a solution is given here for an infinite half space to pulses of finite duration and impulses.

Exponential Impulse Into a Semi Finite Medium

The defining equations are:

$$k\frac{\partial^2 T}{\partial x^2} = \rho c\frac{\partial T}{\partial t} - \dot{q}(x,t)$$

where,

13) $\frac{\partial T}{\partial x}(0) = 0$ (insulated exposed surface)

$$T(\infty,t) = 0$$

$$q(x,t) = \delta(t)\, T_o e^{-\mu x}$$

$$T_o = \frac{\Delta E \mu}{\rho c}$$ where ΔE is the energy in any portion of a spectrum

As demonstrated in part I, this problem has the same solution as

14) $$k\frac{\partial T^2}{\partial x^2} = \rho c\frac{\partial T}{\partial t}$$

where,

$$\frac{\partial T}{\partial x}(0) = 0$$

$$T(\infty,t) = 0$$

$$T(x,o) = T_o\, e^{-\mu x}$$

The solution can be found by performing the integral[10]

$$15)\quad T(x,t) = \frac{1}{2\sqrt{\pi\alpha t}} \int_o^\infty T_o e^{-\mu x'} \left\{ e^{-(x-x')^2/4\alpha t} + e^{-(x+x')^2/4\alpha t} \right\} dx'$$

which yields the following result

$$16)\quad T(x,t) = \frac{T_o}{2} e^{\mu^2\alpha t} \left\{ e^{-\mu x}\left[1 + \operatorname{erf}\left(\frac{x}{2\sqrt{\alpha t}} - \mu\sqrt{\alpha t}\right)\right] + e^{\mu x}\left[1 - \operatorname{erf}\left(\mu\sqrt{\alpha t} + \frac{x}{2\sqrt{\alpha t}}\right)\right]\right\}$$

Although this expression is exact, it cannot be evaluated numerically for the very large values of μ which could be associated with low energy photon irradiation.

Therefore we make use of the explicit evaluation of the error function which is used for computer application.[11] That is,

$$17)\quad \operatorname{erf}(x) = 1 - f(Z)\, e^{-x^2}$$

$$18)\quad f(Z) = a_1 t + a_2 t^2 + a_3 t^3 + a_4 t^4 + a_5 t^5$$

$$t = \frac{1}{1+pZ}$$

p, a_1 - a_5 are constants given in reference 11.

Four cases can now be considered and as a convenience we let

$$B = \mu\sqrt{\alpha t} \qquad C = \frac{x}{2\sqrt{\alpha t}}$$

1. $x = 0$

When equation 17 is substituted into equation 16 the following expression is obtained:

19a) $T(x,t) = T_o\, f(B)$

2. when $C > B$

19b) $T(x,t) = T_o \exp(B^2 - \mu x) + \frac{T_o}{2}\,[f(C+B)-f(C-B)]\, e^{-C^2}$

3. when $B > C$

19c) $T(x,t) = [f(B-C)+f(C+B)]\, e^{-C^2}$

4. when $B = C$

19d) $T(x,t) = \frac{T_o}{2}\, e^{-B^2}\, [1 + f\,(C+B)]$

Equation 19 is used in a form where all the exponential terms are negative and can be evaluated accurately for computer analysis. These equations represent a Green's function in time and can be used to determine the response for any arbitrary temporal pulse shape. The application of these equations to a pulse of finite width and constant amplitude can be found by performing the integral

20) $T(x,t) = \int_o^{\tau_d} \frac{1}{t_d}$ (equation 16) dt'

The result can be obtained by first getting the results for a continuous pulse which is turned on at $t = 0$.

In reference 10 this has been found to be:

$$21)\quad T(x,t) = \frac{2A_o}{k\mu}(\alpha t)^{1/2}\ \text{ierfc}\ \frac{x}{2\sqrt{\alpha t}} - \frac{A_o}{\mu^2 k}\ e^{-\mu x}$$

$$+ \frac{A_o}{2k\mu^2}\left\{ e^{\mu^2\alpha t - \mu x}\ \text{erfc}\ (\mu\sqrt{\alpha t} - \frac{x}{2\sqrt{\alpha t}}) \right.$$

$$\left. + e^{\mu^2\alpha t + \mu x}\ \text{erfc}\ (\mu\sqrt{\alpha t} + \frac{x}{2\sqrt{\alpha t}}) \right\}$$

where $A_o = \frac{\rho C\ T_o}{t_d} = \frac{\Delta E_\mu}{t_d}$ and ierfc = first integral of the complementary error function.

To evaluate this function it is possible to redefine equation 16 as

$$T(x,t) = H(x,t) = \text{equation 16}$$

Equation 21 contains equation 16 as follows:

$$22)\quad T(x,t) = \frac{A_o}{k\mu}\left\{ 2(\alpha t)^{1/2}\ \text{ierfc}\ \frac{x}{2\sqrt{\alpha t}} - \frac{e^{-\mu x}}{\mu} \right\} + \frac{H(x,t)}{\alpha\mu^2 td}$$

Substituting for A_o and $\alpha = k/\rho c$, Equation 22 can be rewritten as:

$$23)\quad T(x,t) = \frac{1}{\alpha\mu^2 td}\left\{ T_o\ \mu\ 2(\alpha t)^{1/2}\ \text{ierfc}\ \frac{x}{2\sqrt{\alpha t}} - T_o\ e^{-\mu x} + H(x,t) \right\}$$

$$= Q(x,t)$$

The solution for a pulse of finite width is simply the superposition of a pulse which starts at t = 0 and continues indefinitely and a pulse of equal and opposite intensity which starts at t = t_d as

24) $T(x,t) = Q(x,t) - Q(x,t-td)$

Equations 23 and 24 can then be used with superposition technique and a cross section library to obtain the response to any general spectrum.

II-B-2. Ion Models

In the deposition section methods were shown by which any deposition can be transformed into the general form of a polynomial with coefficients determined by the energy of the ion. In this section a general response model is developed for such depositions. A solution is first obtained for the response in a semi-infinite medium which is used for transients and finally a result for a slab of finite width using lower order polynomial deposition is obtained for an arbitrary number of pulses.

II-B-2-a. General Deposition in a Semi-Infinite Medium

The general solution for any deposition function can be obtained from the theory of Green's functions as:

$$25)\quad T(x,t) = \int_{t'} \int_{x'} \frac{f(t')}{\rho c}\, g(x')\, G(x,t,x',t')\, dx'\, dt'$$

where

$f(t')\, g(x') = \dot{q}(x;t')$ = volumetric energy deposition rate

ρ = density

c = specific heat

and

$G(x,t,x',t')$ = the Green's function which for a semi-infinite slab is:

$$26)\quad G = \frac{1}{2\sqrt{\alpha(t-t')}\sqrt{\pi}} \left\{ e^{-(x'-x)^2/4\alpha(t-t')} + e^{-(x'+x)^2/4\alpha(t-t')} \right\}$$

where α = thermal diffusivity.

The Green's function can be written

$$27)\quad G = \frac{1}{\sqrt{\pi}A}\left\{e^{-(x'-x)^2/A^2} + e^{-(x'+x)^2/A^2}\right\}$$

$$A = 2\sqrt{\alpha(t-t')}$$

since the variables are separable equation 25 can be written

$$28)\quad T(x,t) = \int_{t'} \frac{f(t')}{\rho c} \int_{x'} g(x')G(x,t,x',t')\, dx'\, dt'$$

Before addressing any particular problem such as deposition of energetic ions, a general solution will be developed for spatial distributions of the form

$$29)\quad g(x) = C_0 + C_1x + C_2x^2 + C_3x^3 + C_4x^4$$

where C_i are in general functions of time.

The spatial integral becomes the evaluation of the following sequence

$$S_n = \int$$

$$30)\quad S_N = \frac{C_N}{\sqrt{\pi}} \int\left(\frac{x'^N}{A} e^{-(x'-x)^2/A^2} + \frac{x^N}{A} e^{-(x'+x)^2/A^2}\right) dx'$$

we make use of the following integral,

$$31)\quad \int x^N e^{-a^2x^2+bx}\,dx = \left| a^{-N-1} e^{b^2/4a^2} \sum_{k=0}^{N} \frac{N!}{k'(N-k)!} \left(\frac{b}{2a}\right)^{N-k} \int u^k e^{-u^2} du \right| = III$$

where $ax - b/_{2a} = u$

If the square is completed

$$\int x^N e^{-a^2x^2+bx-b^2/4a^2}\,dx = e^{-b^2/4a^2}\ III$$

then

$$32)\quad \int x^N e^{-(ax-b/2a)^2}\,dx = a^{-N-1} \sum_{k=0}^{N} \frac{N!}{k!(N-k)!} \left(\frac{b}{2a}\right)^{N-k} \int u^k e^{-u^2} du$$

The higher order integrals can now be expressed in terms of the first two (we will now ignore the constant terms $C_i/\sqrt{\pi}$). The integrals can now be represented as:

$$33)\quad S_N = \int \frac{x'^N}{A} e^{-\left(\frac{x'}{A} - \frac{x}{A}\right)^2} dx' + \int \frac{x'^N}{A} e^{-\left(\frac{x'}{A} + \frac{x}{A}\right)^2} dx'$$

If the following convention is adopted

$$S_N = S_N^{(-)} + S_N^{(+)}$$

we have the form of equation (32) with

for $S_N^{(-)}$ $\quad a = \frac{1}{A} \qquad \frac{b}{2a} = \frac{x}{A}$

for $S_N^{(+)}$ $\quad a = \frac{1}{A} \qquad b/2a = -\frac{x}{A}$

evaluating the S_N's

$$S_o^{(\bar{+})} = \int e^{-u^2}\, du = \int \frac{1}{A}\, e^{-\left(\frac{x'}{A} \bar{+} \frac{x}{A}\right)^2} dx' = I_o(\bar{+})$$

if $\quad u = \frac{x'}{A} \bar{+} \frac{x}{A}$

$$S_1^{(\bar{+})} = \frac{1}{A} A^2 \left\{ \left(\pm \frac{x}{A}\right) \int e^{-u^2}\, du + \left(\pm \frac{x}{A}\right)^o \int u'\, e^{-u^2}\, du \right\}$$

which can be expressed as

$$S_1^{(\bar{+})} = \pm x\, I_o + A\, I_1$$

likewise

$$S_2^{(\bar{+})} = (\pm x)^2\, I_o + 2(\pm x)\, A\, I_1 + A^2\, I_2$$

$$S_3^{(\bar{+})} = (\pm x)^3\, I_o + 3(\pm x)^2 A I_1 + 3\,(\pm x)\, A^2 I_2 + A^3 I_3$$

$$S_4^{(\bar{+})} = (\pm x)^4\, I_o + 4\,(\pm x)^3\, A I_1 + 6(\pm x)^2\, A^2\, I_2 + 4(\pm x)\, A^3 I_3 + A^4 I_4$$

Summarizing

$$S_N^{(\bar{+})} = \int \frac{x'^N}{A}\, e^{-\left(\frac{x'}{A} \bar{+} \frac{x}{A}\right)^2} dx'$$

which can be expressed in matrix form as

N	I_o	I_1	I_2	I_3	I_4
0	1				
1	$\pm x$	A			
2	$(\pm x)^2$	$2(\pm x)A$	A^2		
3	$(\pm x)^3$	$3(\pm x)^2A$	$3(\pm x)A^2$	A^3	
4	$(\pm x)^4$	$4(\pm x)^3A$	$6(\pm x)^2A^2$	$+ 4(\pm x)A^3$	A^4

34)

in order to evaluate the I_N's the following convention is adopted

$$I_N^- = \int \left(\frac{x'}{A} - \frac{x}{A}\right)^N e^{-\left(\frac{x'}{A} - \frac{x}{A}\right)^2} dx'$$

$$I_N^+ = \int \left(\frac{x'}{A} + \frac{x}{A}\right)^N e^{-\left(\frac{x'}{A} + \frac{x}{A}\right)^2} dx'$$

The solution can be rewritten (by adding $S^{(+)}$ and $S^{(-)}$)

$$S_o = [I_o^- + I_o^+]$$

$$S_1 = x\,[I_o^- - I_o^+] + A\,[I_1^- + I_1^+]$$

35) $$S_2 = x^2\,[I_o^- + I_o^+] + 2xA\,[I_1^- - I_1^+] + A^2\,[I_2^- + I_2^+]$$

$$S_3 = x^3\,[I_o^- - I_o^+] + 3x^2A\,[I_1^- + I_1^+] + 3xA^2\,[I_2^- - I_2^+] + A^3\,[I_3^- + I_3^+]$$

$$S_4 = x^4\,[I_o^- + I_o^+] + 4x^3A\,[I_1^- - I_1^+] + 6x^2A^2[I_2^- + I_2^+] + 4xA^3\,[I_3^- - I_3^+] + A^4\,[I_4^- + I_4^+]$$

The complete solution to equation 28 is then

36) $T(x,t) = \int_{t'} dt \frac{f(t')}{\rho c} \frac{1}{\sqrt{\pi}} \left[C_o S_o + C_1 S_1 + C_2 S_2 + C_3 S_3 + C_4 S_4\right]$ evaluated at limits of x'

I_N's can be evaluated in the following manner:

$$I_o = \int e^{-u^2} du = \frac{\sqrt{\pi}}{2} \text{ erf } (u)$$

$$I_1 = \int u\, e^{-u^2} du = \frac{-1}{2} e^{-u^2}$$

and knowing $\int u^N e^{-u^2} du = -\frac{1}{2} u^{N-1} e^{-u^2} + \frac{N-1}{2} \int u^{N-2} e^{-u^2} du \quad (N \geq 2)$

$$I_2 = -\frac{1}{2} u\, e^{-u^2} + \frac{1}{2} I_o = -\frac{1}{2} F_1 + \frac{1}{2} I_o$$

$$I_3 = -\frac{1}{2} u^2 e^{-u^2} + I_1 = -\frac{1}{2} F_2 + I_1$$

$$I_4 = -\frac{1}{2} u^3 e^{-u^2} + \frac{3}{2} \int u^2 e^{-u^2} du = -\frac{1}{2} F_3 - \frac{3}{4} F_1 + \frac{3}{4} I_o$$

in terms of I_o, I_1 and F_N this may be summarized

I_N	I_o	I_1	F_1	F_2	F_3
I_o	1				
I_1		1			
I_2	1/2		-1/2		
I_3		1		-1/2	
I_4	3/4		-3/4		-1/2

where $F_N = u^N e^{-u^2}$

Equation 36 and 34 may be combined to give a general result

$$37)\quad T(x,t) = \int dt' \frac{f(t')}{\rho c} \frac{1}{\sqrt{\pi}} \sum C_N S_N \Bigg|_{\text{limits of } x'} \quad \text{evaluated at}$$

where

S_N are the diagonal terms ($S_N \rightarrow$ NNth term) of the matrix product

$$|Q| \quad |M|$$

where $|Q|$ is

$$38)\quad \begin{vmatrix} 1 & & & & \\ x & A & & & \\ x^2 + A^2/2 & 2xA & \frac{-A^2}{2} & & \\ \frac{3A^2x}{2} + x^3 & 3x^2A + A^3 & \frac{-3xA^2}{2} & \frac{-A^3}{2} & \\ \frac{3A^4}{4} + \frac{6A^2}{2}x^2 + x^4 & 4xA^3 + 4x^3A & \frac{-6A^2}{2}x^2 - \frac{3A^4}{4} & \frac{-4xA^3}{2} & -\frac{A^4}{2} \end{vmatrix}$$

and $|M|$ is

$$39)\quad \begin{vmatrix} I_0(+) & I_0(-) & I_0(+) & I_0(-) & I_0(+) \\ & I_1(+) & I_1(-) & I_1(+) & I_1(-) \\ & & F_1(+) & F_1(-) & F_1(+) \\ & & & F_2(+) & F_2(-) \\ & & & & F_3(+) \end{vmatrix}$$

where $I_N(+) = (I_N^- + I_N^+)$

$I_N(-) = (I_N^- - I_N^+)$

Equation 37 represents a general solution for any deposition interval when the functions are contained are evaluated at the limits of the region in which the polynomial applies. Substitution of the limits can simplify the result when the symmetry of the functions I_N and F_N are accounted for. The following relations are noted:

$$I_o = \sqrt{\pi}/2 \ \mathrm{erf}(u) = \text{odd}$$

$$I_1 = -\frac{1}{2} e^{-u^2} = \text{even}$$

40) $$F_1 = u\, e^{-u^2} = \text{odd}$$

$$F_2 = u^2 e^{-u^2} = \text{even}$$

$$F_3 = u^3 e^{-u^2} = \text{odd}$$

when the limits $0 \rightarrow x_m$ are inserted into equation 35 the $|M|$ matrix is transformed as:

$$|M|_{LIMITS} = |M_L| =$$

41)
$$\begin{vmatrix} I_o(+) & I_o(-) + 2\, I_o(o) & I_o(+) & I_o(-) + 2\, I_o(o) & I_o(+) \\ & I_1(+) - 2\, I_1(o) & I_1(-) & I_1(+) - 2\, I_1(o) & I_1(-) \\ & & F_1(+) & F_1(-) + 2\, F_1(o) & F_1(+) \\ & & & F_2(+) - 2\, F_1(o) & F_2(-) \\ & & & & F_3(+) \end{vmatrix}$$

where $I_N(+) - 2\, I_N(o)$ is to be interpreted as $I_N(\frac{x_m - x}{A}) + I_N(\frac{x_m + x}{A}) - 2\, I_N(0 + \frac{x}{A})$

Finally, a general solution is obtained when equation 37 is evaluated. The spatial contribution is contained in the evaluation of the function $\Sigma\ C_N S_N$ at the limits of the deposition region while the temporal contribution is done numerically to accommodate arbitrary spectra.

If the deposition does not require all five coefficients, the formulation is of course much simpler. The solution given in part I is actually the same as equation 37 if the coefficients C_2, C_3, C_4, $C_5 = 0$, which corresponds to an ion in region I with equation 1 chosen for the deposition. The equation is simplified as the matrices $|Q|$ and $|M|$ become:

$$|Q| = \begin{vmatrix} 1 & \\ x & A \end{vmatrix}$$

42)
$$|M| = \begin{vmatrix} I_o(+) & I_o(-) \\ & I_1(+) \end{vmatrix}$$ evaluated at limits of region

The uniform deposition model, which was appropriate for some high mass-low energy ions, would result in an even more simplified result where

43)
$$|Q| = |1|$$

$$|M| = |I_o(+)|$$

In summary, the complete solution for an ion which requires deposition functions in all regions (I, II, III) can then be expressed.

$$44)\quad T(x,t) = \int_{t'} \frac{f(t')}{\rho c}\,\frac{dt'}{\sqrt{\pi}} \left\{ \sum_{N=0}^{4} C_{1N} S_N \Big|_{\text{limits of region III}} + \sum_{N=0}^{4} C_{2N} S_N \Big|_{\text{limits of region II}} + \sum_{N=0}^{4} C_{3N} S_N \Big|_{\text{limits of region I}} \right\}$$

where S_N are the NN elements of $|Q|$ (equation 38)
and $|M|$ (equation 39)

$|Q|$ and $|M|$ consist of the functions

$$I_o = \frac{\sqrt{\pi}}{2}\ \mathrm{erf}(u)$$

$$I_1 = -1/2\ e^{-u^2}$$

$$F_1 = u\ e^{-u^2}$$

$$F_2 = u^2\ e^{-u^2}$$

$$F_3 = u^3\ e^{-u^2}$$

and the elements of eqn. 39 are interpreted as

$$I_N(+) = I_N\left(\frac{x'-x}{A}\right) + I_N\left(\frac{x'+x}{A}\right)$$

$$I_N(-) = I_N\left(\frac{x'-x}{A}\right) - I_N\left(\frac{x'+x}{A}\right)$$

where $A = 2\sqrt{\alpha(t-t')}$

II-B-2-b. Ion Deposition in Finite Slabs

The formulation for the temperature response for a series of ion pulses is best developed for a finite width material since the sustained value of the temperature will be more directly influenced by a boundary condition at the rear surface. The same semi-infinite solution presented above would still, however, be used to evaluate the transients which are not influenced by the rear boundary.

For the case in which a radiation pulse train is incident on a slab of material, a solution can be developed for two simple deposition models: a uniform deposition and a linearly decreasing model. The procedure is easily extended to more general deposition models. At any given time the spatial deposition will be given by either of the two functions shown in figure 12. These functions will vary for arbitrary spectra but their general shape will be the same.

The problem for a single group of ions which contains $f(t')\,dt'$ ions can be stated as

$$k \frac{\partial^2 T}{\partial x^2} = \rho c \frac{\partial T}{\partial t}$$

45)

$$\frac{\partial T}{\partial x} = (0,t) = 0$$

$$T(x,0) = f(x)/\rho c = f(x)$$

$$T(L,t) = 0 \quad \text{(constant temperature rear surface)}$$

This has the solution[10]

Figure 12
Deposition Models

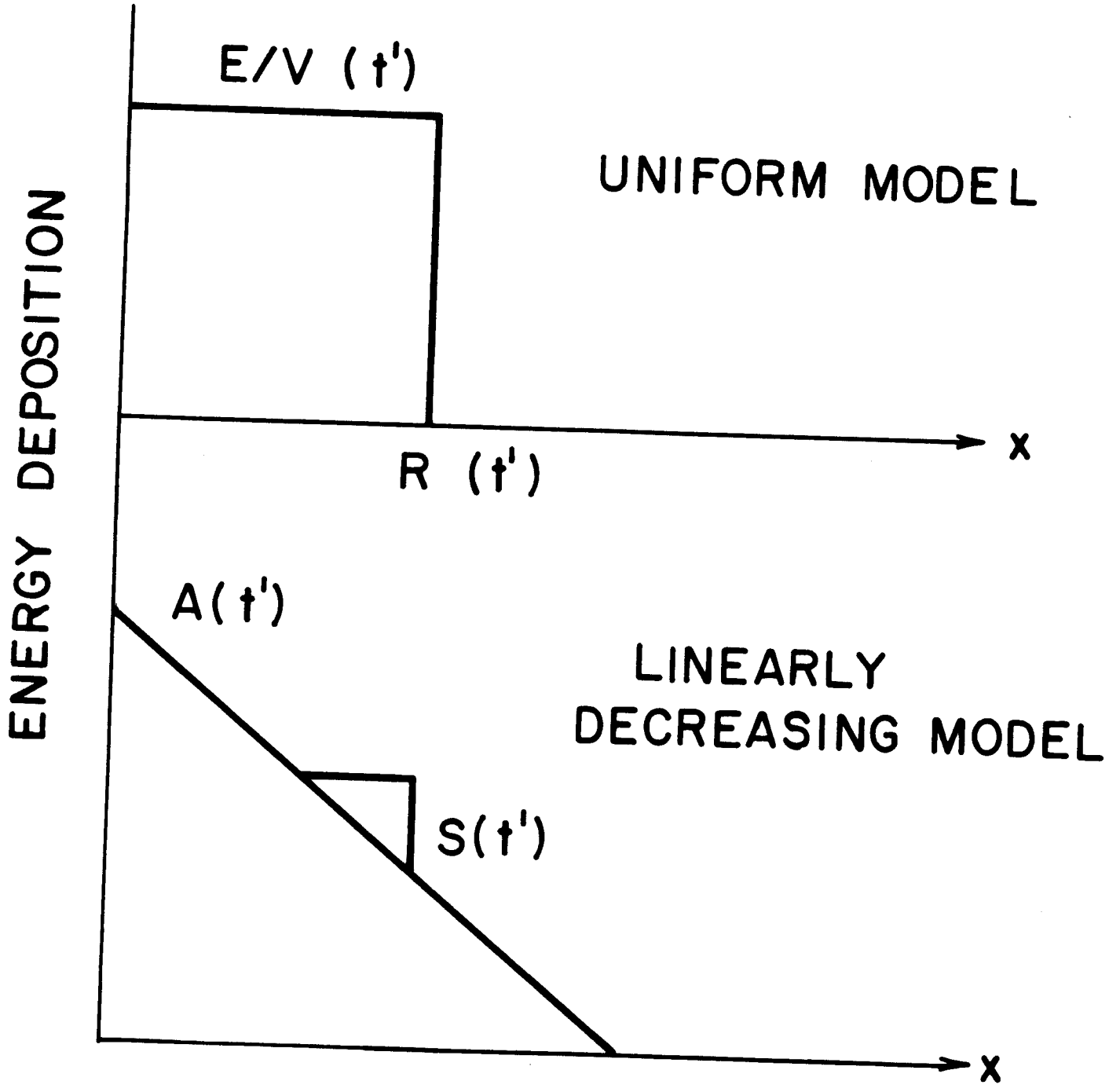

$$46)\quad T(x,t) = \sum_{N=1}^{\infty} \cos B_N \frac{x}{L}\, e^{-B_N^2\theta}\, \frac{2}{L} \int_0^L f(x) \cos \frac{B_N x}{L}\, dx$$

where $B_N = (2N-1)\pi/2$ $\qquad \theta = \alpha t/L^2$

α = thermal diffusivity

L = slab width

Equation 46 has the form

$$47)\quad T(x,t) = \sum_{N=1}^{\infty} A(Z)\, e^{-B_N^2\theta}\, B(Z)$$

where $Z = x/L$

The solution to this same group for a series of pulses as shown in figure 13 can be obtained by Laplace transforms, similar to the method employed in part I for multiple photon irradiations.

In this case the transfer function is the transform of equation 45

$$48)\quad H(S) = \sum_{N=1}^{\infty} A(Z)\, B(Z)\, \frac{1}{S + \frac{B_N^2\alpha}{L}}$$

The transform of the solution for a series of M pulses can be obtained by convolution since the transform of a series of impulses is

$$49)\quad V(S) = 1 + e^{-\omega s} + e^{-2\omega s} + - - -$$

then

$$50)\quad T(x,t) = \mathscr{L}^{-1}\, H(s)\, V(s)$$

which as shown in part I is

$$51)\quad T(x,t) = \sum_{N=1}^{\infty} A(Z)\, B(Z)\, e^{-B_N^2\theta} \left[\frac{1 - e^{-B_N^2\gamma\, M}}{1 - e^{-B_N^2\gamma}}\right]$$

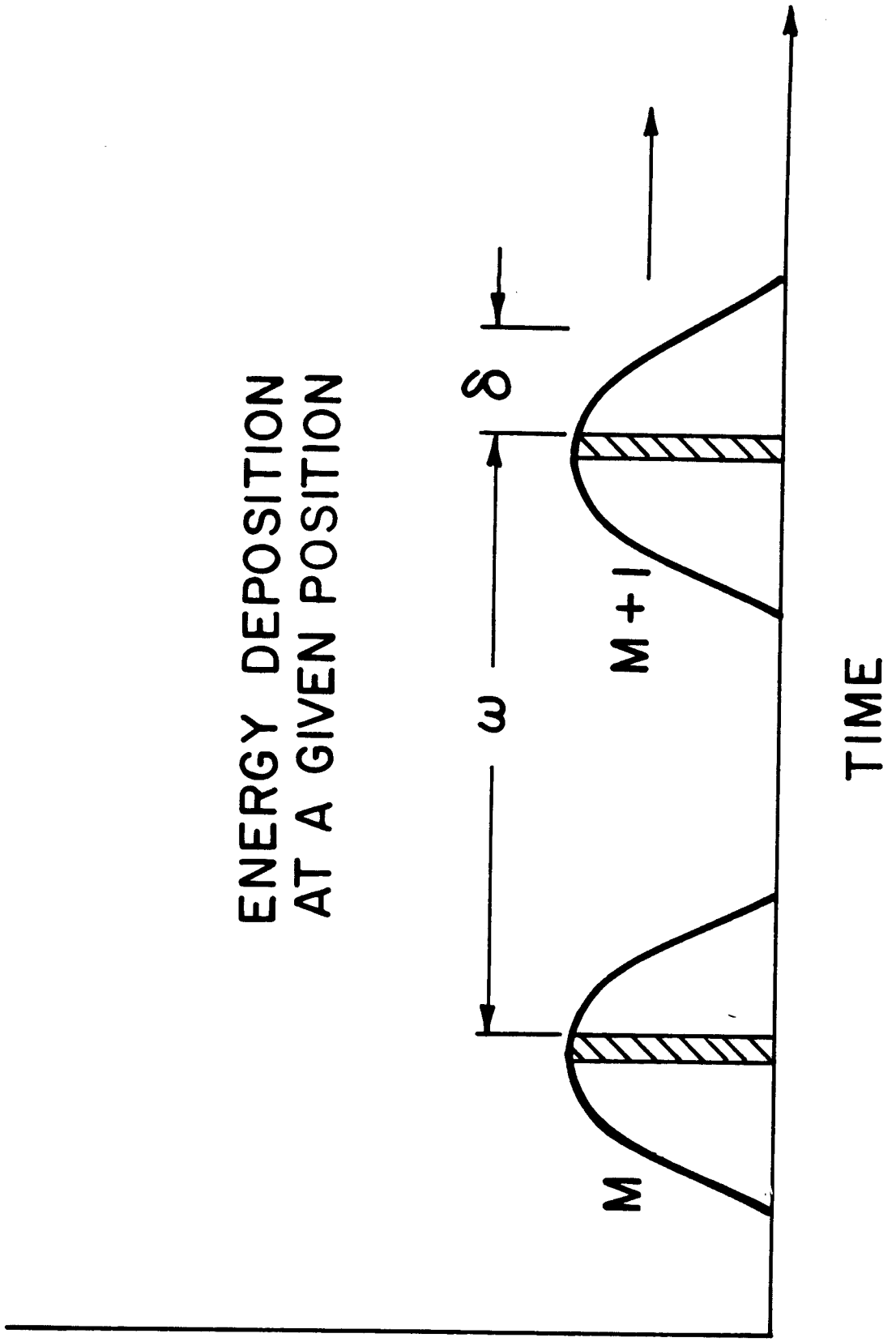
ENERGY DEPOSITION, E/V
ENERGY DEPOSITION
AT A GIVEN POSITION
δ
ω
M+1
M
TIME

Figure 13

where $\theta = \frac{\alpha\delta}{L^2}$ $\gamma = \frac{\alpha\omega}{L^2}$

M = # of pulses

δ = time from last impulse

In a linear system equation 51 becomes a composite (meaning the response to all previous impulses) Green's function for M impulses.

The response at time t measured from the start of the M'th pulse (figure 13) can be determined from the theory of Green's functions as

$$52) \quad T(x,t) = \int_0^{t^*} G(x,t,t')\, dt'$$

where $t^* = t \qquad t < t_{max}$

$t^* = t_{max} \qquad t > t_{max}$

and consideration of equation 51, the Green's function is actually just

$$53) \quad G(x,t,t') = \sum_{N=1}^{\infty} A(Z)\, B(t',Z)\, e^{-B_N^2\theta} \left[\frac{1 - e^{-B_N^2\gamma M}}{1 - e^{-B_N^2\gamma}}\right]$$

B is a function of t' since in general the limits of the integration over space will be a function of ion arrival time as

$$\theta = \frac{\alpha(t-t')}{L^2}$$

At this point it is necessary to determine the function B for the spatial profile considered. B was defined in equation 47 as

$$54) \quad B(t',x) = \frac{2}{L} \int_0^L f(x) \cos B_N \frac{x}{L}\, dx$$

If the uniform deposition profile of figure 12 is used for f(x) this becomes

$$55) \quad B(t',x) = \frac{2}{L} \int_0^{R(t')} \frac{F(t')}{R(t')\rho c} \cos B_N x/L \, dx$$

where R(t') is the end of the deposition region. This yields the result

$$56) \quad B(t',x) = 2 \frac{F(t')}{R(t')\rho c} \frac{1}{B_N} \sin \frac{B_N R}{L}$$

where F(t') is the energy unit area in the interval dt'.

Equation 56 can then be put in equations 53 and 52 to obtain the solution for an entire spectrum of particles.

If the linearly decreasing deposition profile (figure 12) is chosen equation 54 becomes

$$57) \quad B(t',x) = \frac{2}{L} \int_0^{A(t')/S(t')} \frac{A(t') - S(t')x}{\rho c} \cos \frac{B_N x}{L} \, dx$$

where A(t') - S(t')x represents the energy per unit volume in the interval dt'. The result of this integration is

$$58) \quad B(t',x) = \frac{2 L S(t')}{B_N^2} \left[1 - \cos \frac{B_N A(t')}{S(t') L}\right]$$

Equation 58 can likewise be put into equation 53 and 52 to obtain a solution for a spectrum of particles.

II-C. Stress Response

In part I the defining equations for the generation of thermoelastic stress waves in elastic media were presented. This section will address the solution of these equations and consider the temporal or spatial criteria necessary for establishment of a stress wave of significant amplitude from the transient deposition of energy.

The procedure will be to pick a deposition model, derive a set of equations for the temperature and stress responses and then examine the relation between the deposition depths and times which produce stress waves.

The emphasis will be on deriving the time scales over which energy must be deposited for wave generation. The result will be to establish that middle ground between the "instantaneous" deposition of energy which occurs faster than the material can expand thus producing stress waves and the slow heating of a specimen which produces an equilibrium expansion and does not generate stress waves in a one dimensional strain configuration.

An example of a particular deposition pulse is chosen which can be characterized in both time and space and which is similar to that encountered in ion irradiations.

Problem Statement

Consider a pulse of energy which arrives at the surface of a semi-infinite media (Figure 14).

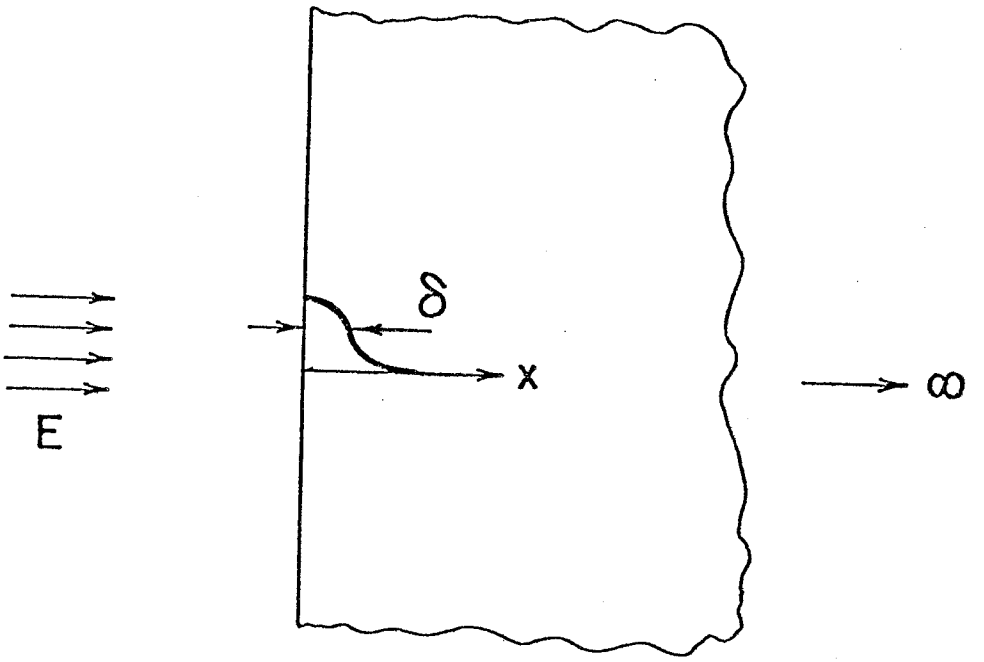

Figure 14

Problem Statement

The energy will penetrate into the material with some characteristic depth, δ, and will have a time history given by some function f(t) which will have some characteristic width, θ. If θ is sufficiently small a stress wave will be generated which will propagate into the material. The wave will have a wave length of the order of δ and will propagate with some velocity, c, in the media.

Let us consider an energy pulse with the following characteristics, a volumetric heating rate given by:

59) $\dot{q}(x,t) = f(t)\, g(x)$

60) where $g(x) = \frac{E}{\sqrt{2\pi}\ \delta}\ e^{-1/2(\frac{x}{\delta})^2}$

61) and $f(t) = \omega \sin \omega t$

so in space the function is gaussian with characteristic width, δ, as

Figure 15

Spatial Profile

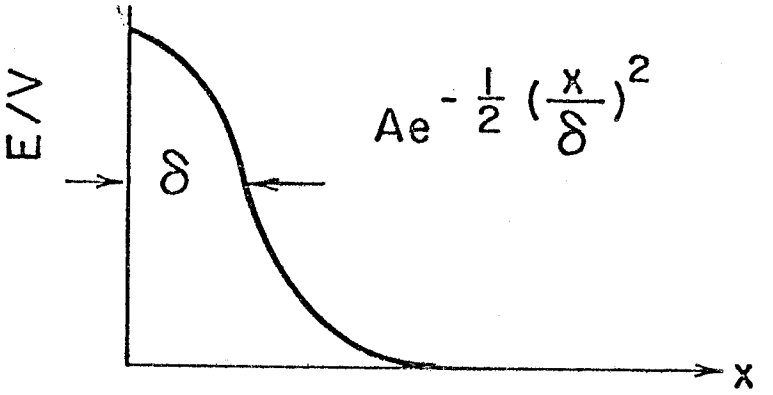

and in time

Figure 16

Time History

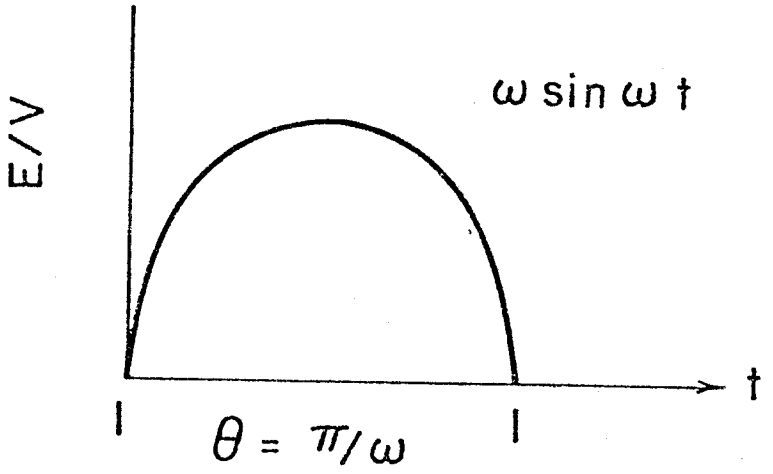

the integral over all space and time is seen to be

$$\int_0^{\pi/\omega}\int_0^{\infty} f(t)\,g(x) = \int_0^{\pi/\omega} \frac{1}{2} E\omega \sin \omega t = E \left\{ \begin{matrix} \text{the energy} \\ \text{in the} \\ \text{pulse} \end{matrix} \right\}$$

The defining equation for the stress response as shown in part I is

62) $$\frac{\partial^2 \sigma}{\partial x^2} - \frac{1}{c^2}\frac{\partial \sigma}{\partial t^2} = A\frac{\partial^2 T}{\partial t^2}$$

$$c = \frac{E/\rho\,(1-\nu)}{(1+\nu)(1-2\nu)}$$ longitudinal wave velocity

$$A = \rho\alpha \frac{(1 + \nu)}{(1 - \nu)}$$

α = coefficient of thermal expansion (linear)

The temperature response is given as in the previous section as

63) $$k \frac{\partial^2 T}{\partial x^2} = \rho c \frac{\partial T}{\partial t} - \dot{q}(x,t)$$

METHOD OF SOLUTION

The equations to be solved are 62) and 63). The equations are coupled since the wave equation is driven by the temperature equation, but the temperature equation is independent so in a true sense this represents an uncoupled solution.

The procedure used here will be to assume that temperature diffusion is a "slower" process than wave propagation and hence the times of interest for the wave equation are short compared to the thermal response.

We will first solve the temperature equation completely and determine the deposition times in which the response is adiabatic, that is, when the temperature is given by:

64) $$\frac{\partial T}{\partial t} = \frac{\dot{q}(x,t)}{\rho c}$$

in this case the temperature field is completely known, for short times, and its time dependence is given by the chosen energy deposition function, f(t) - eqn. 61.

We will then solve the stress equation and examine the amplitude of the stress wave as a function of the characteristic deposition times. If the amplitude of the stress wave approaches zero while the deposition times are still short enough for the adiabatic assumption to be valid then the original assumption was valid and the solution is accurate.

TEMPERATURE SOLUTION

The equation to be solved* is

65) $$k \frac{\partial^2 T}{\partial x^2} + \frac{E\omega}{\sqrt{2\pi}\delta} \sin \omega t \; e^{-x^2/\delta^2} = \rho c \frac{\partial T}{\partial t}$$

subject to

$$\frac{\partial T}{\partial x} = 0 \qquad \text{at} \qquad x = 0$$

$$T \to 0 \qquad \text{as} \qquad x \to \infty$$

The solution can be obtained by a Green's function technique similar to that employed in the previous section with the following result:

66) $$T(x,t) = \int_0^{\pi/\omega} T_0 \frac{1}{\sqrt{1+y}} e^{-z^2/(1+y)} \sin \omega t' \, dt'$$

where

$$y = \frac{4\alpha(t - t')}{\delta^2}, \qquad z = x/\delta$$

α = thermal diffusivity $\qquad T_0 = \dfrac{E\omega}{\sqrt{2\pi}\,\delta\,\rho c}$

If $\theta = \pi/\omega$ is very small, the problem will be adiabatic, and the solution for temperature will be the solution to equation 64) which by simple integration is:

67) $$T^*(x,t) = \int_0^{MIN(t,\pi/\omega)} T_0 \sin \omega t \; e^{-z^2} \, dt$$

$$T^*(x,t) = (1 - \cos \omega t)\frac{T_0}{\omega} e^{-z^2}$$

---

*This temperature solution is specific for a gaussian energy deposition and was chosen to illustrate the coupling of temperature and stress response. The general temperature is given in section II-B.

The next step is to evaluate and compare the solution to Eqs. (66) and (67) so that we may determine which times (θ's = π/ω) are actually short enough to be considered adiabatic. These equations were incorporated into a computer program and were evaluated for various values of θ and τ, where θ is the deposition time and τ is the time at which the response is evaluated, as shown in figure 17.

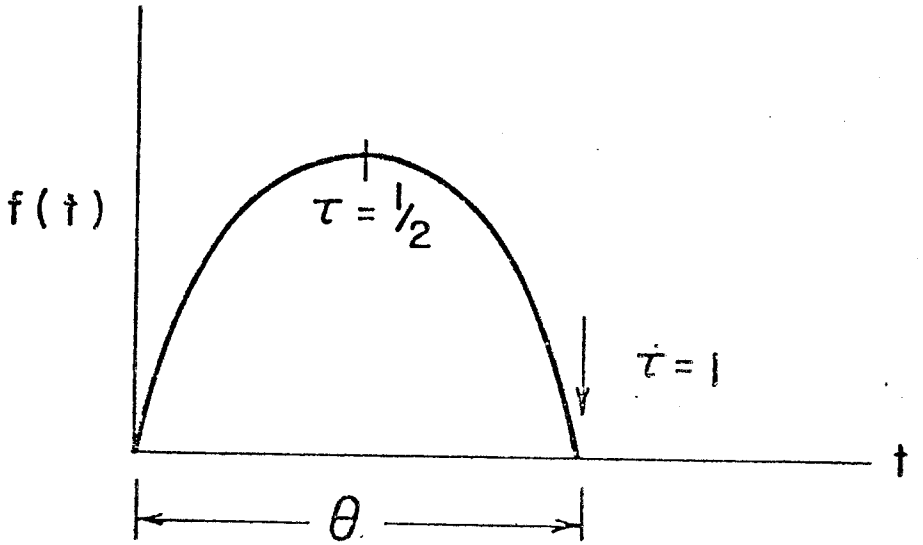

Figure 17
Time Constants

The solution for θ's between 10^{-11} and 10^{-5} are given in Figure 18 a,b,c for three values of x for α = .1, $\delta = 10^{-4}$. Data are shown in terms of T/T* for τ = 1/2 and 1.

It is seen in Figure 18 that for this case the response is essentially adiabatic (within 10%) for pulse durations (θ's) up to about 10^{-8} seconds at least out to x values of δ.

Figure 18
Transient Temperature Response

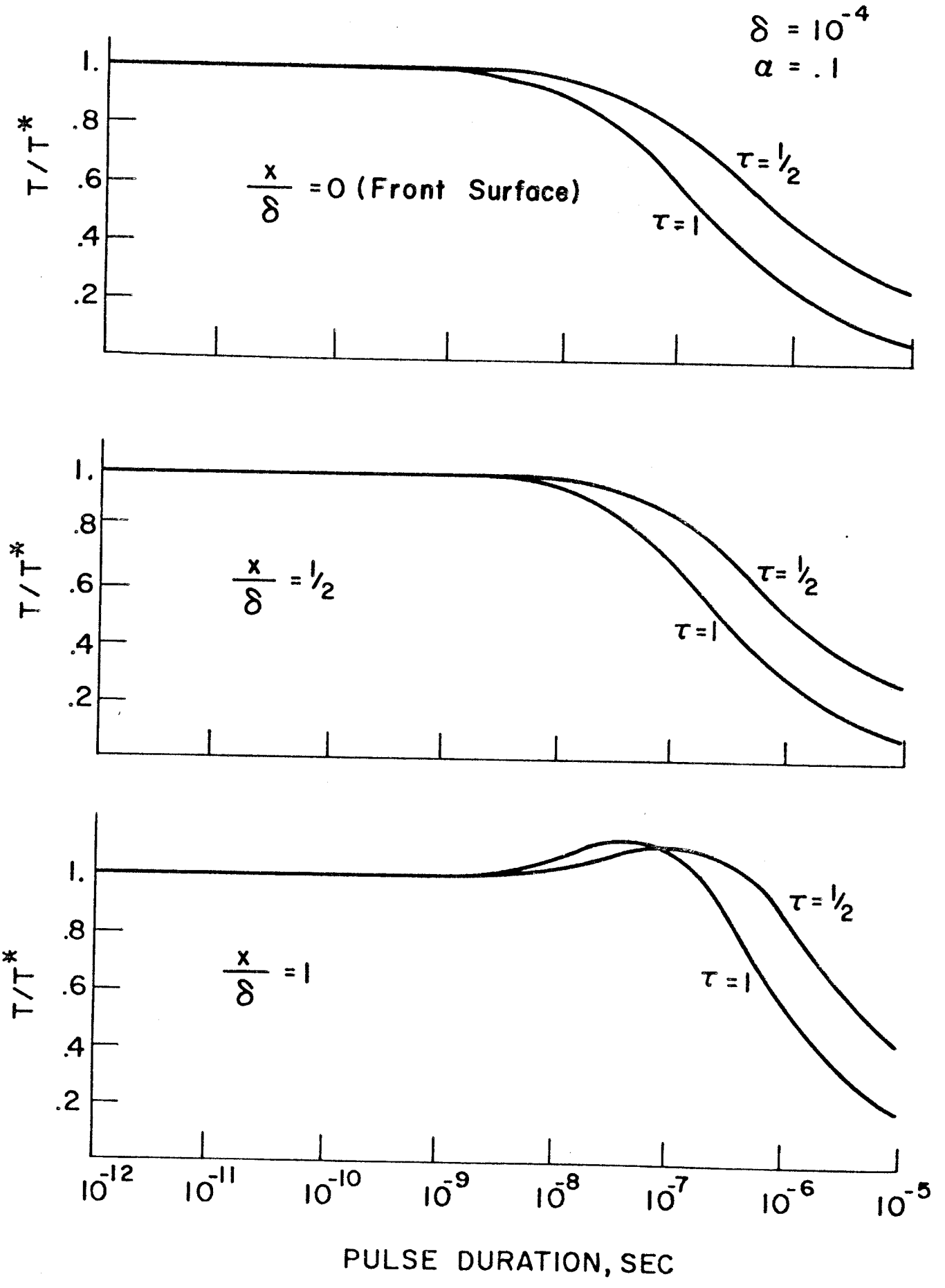

Where, as in equation (66),

$$y = \frac{4\alpha t}{\delta^2} = \frac{4(.1)(10^{-8})}{(10^{-4})^2} = .4$$

or

$$y = \text{order}(1)$$

During pulses with duration $\theta < 10^{-8}$ sec, the temperature solution is given by Eq. (67), and if we find that the durations for stress wave generation are smaller than these, then Eq. (67) will always be a good approximation for $T(x,t)$.

As a reference for numerical values, for the sample problem above, the defining parameters were:

Thermal diffusivity = .1 cm^2/sec

$$\delta = 1 \times 10^{-4} \text{ cm}$$

$$E = .1 \text{ J/cm}^2$$

$$\rho c = 1 \text{ J/°C cm}^3$$

The adiabatic temperature at x = 0 for very short times is:

$$T_{MAX} = 796°C$$

STRESS SOLUTION

Equation (62)

$$\frac{\partial^2\sigma}{\partial x^2} - \frac{1}{c^2}\frac{\partial^2\sigma}{\partial t^2} = \frac{\partial^2 T}{\partial t^2}\rho\alpha\frac{(1+\nu)}{(1-\nu)}$$

can be coupled with the constitutive relation for uniaxial strain

68) $$\sigma = \frac{eE(1-\nu)}{(1+\nu)(1-2\nu)} - \frac{E\alpha}{(1-2\nu)}T$$

where e = strain

to set up a solution for the stress. Consider the case of an impulse of energy deposition which has spatial form g(x). This deposition will result in an adiabatic temperature change as discussed above.

It will also result in a stress increase, since it will happen in a time too short for the material to expand. The resulting stress profile will be

69) $$\sigma(x) = \left(\frac{E\alpha}{1 - 2\nu}\right)T(x) = \gamma T(x)$$

The response of Eq. (62) in this case must be the same as the solution to the homogeneous wave equation with the initial condition of Eq. (69). The solution of the wave equation of the form

70) $$\frac{\partial^2\phi}{\partial x^2} - \frac{1}{c^2}\frac{\partial^2\phi}{\partial t^2} = 0$$

with boundary condition

$$\phi(0,t) = 0$$

and initial conditions

$$\phi(x,0) = \phi_0(x)$$

$$\left.\frac{\partial\phi}{\partial t}\right]_{t=0} = V_0(x)$$

is the D'Alemberts solution which is [12]

71) $$\phi(x,t) = \frac{1}{2}P(x - ct) + \frac{1}{2}P(x + ct) + \frac{1}{2c}\int_{x-ct}^{x+ct} Q(\zeta)d\zeta$$

where

$$P(x) = \begin{cases} \phi_0(x) & x \geq 0 \\ -\phi_0(-x) & x < 0 \end{cases}$$

$$Q(x) = \begin{cases} V_0(x) & x \geq 0 \\ -V_0(-x) & x < 0 \end{cases}$$

In our case,

$$V_0(x) \equiv 0$$

$$\phi_0 = \gamma T(x)$$

hence the solution is:

72) $$\sigma_I(x,t) = \frac{1}{2}[\, T(x - ct)H(x - ct) - \gamma T(ct - x)H(ct - x) + \gamma T(x + ct)]$$

where

$H(y)$ is the step function.

Equation (72) represents the solution for a single impulse of energy. The general time-dependent deposition problem may be treated by recognizing that any pulse is a summation of many impulses as in figure 19.

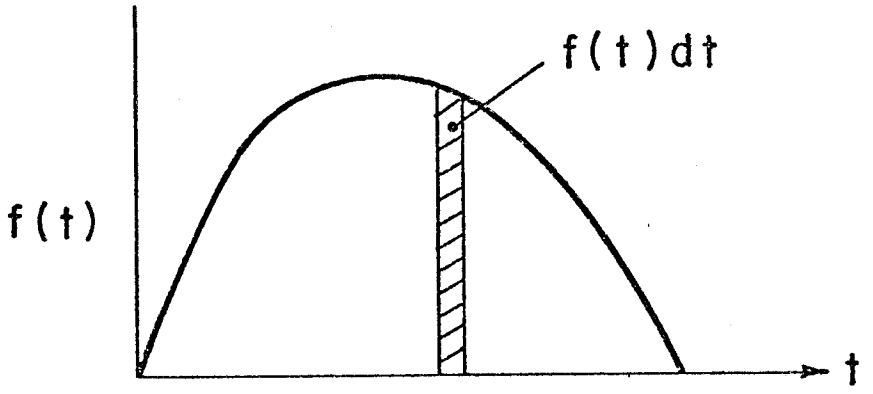

Figure 19. Deposition Pulse

Hence, a general solution is found by recognizing that the system is linear and summing over all the impulses in the time-dependent deposition, which the time variable is replaced by the physical time minus the time the impulse occurred as:

73) $$\sigma(x,t) = \sum f_i(t)dt_i \quad \sigma_I(x,t - t_i)$$

or

74) $$\sigma(x,t) = \int_{t'} \sigma_I(x,t - t')f(t')dt'$$

where σ_I is given by Eq. (72), and

$$T(x) = T_o\, e^{-z^2}$$

Equations (72), (73), and (74) were derived on a semi-intuitive basis and may seem somewhat unsatisfying. As a result, a rigorous solution of the inhomogeneous wave equation for this case is obtained and presented in Appendix A. The resulting solutions are identical to those developed here.

Equation 74 is similiar in concept to that of Zaker[13] but was developed here in the form of a general Green's function which could be applied to the energy depositions anticipated in transient ion irradiations of arbitrary spectra. This form of solution will now be used to determine the radiation conditions which must be met for stress waves to develop.

If the deposition time were very short, the temperature response would be adiabatic and the stress response would at the end of the pulse be given by:

75) $$\sigma^*(x,\theta) = \gamma T^*(x,\theta) = \gamma\, 2\, \frac{T_0}{\omega}\, e^{-z^2}$$

which would look like that of Figure 20

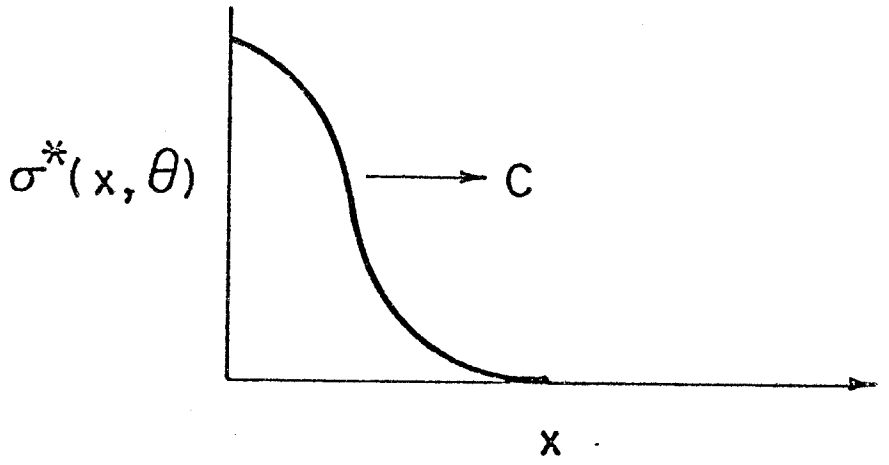

Figure 20. Initial Stress Wave From Impulse Deposition

This stress profile will then propagate into the material and be modified by a rarefaction wave which proceeds from the free surface so that at large distances into the material the profile will look like that in figure 21.

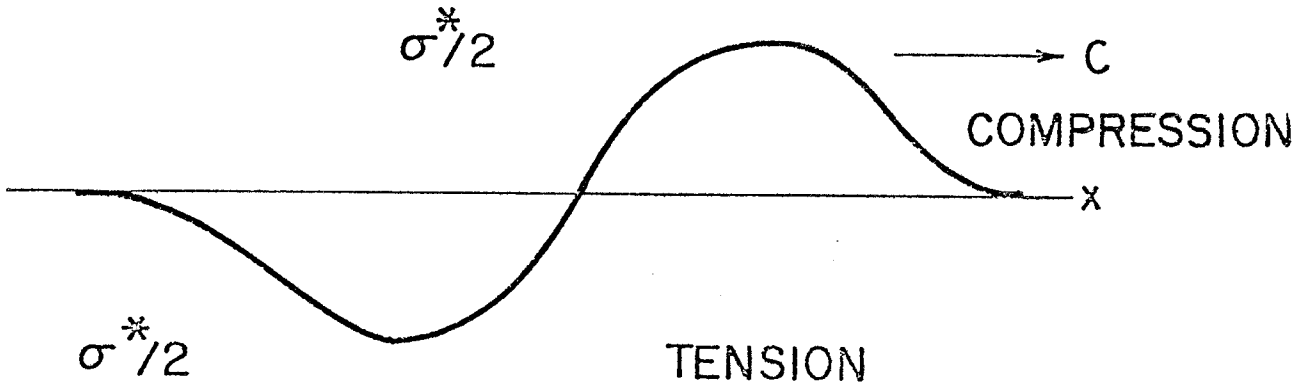

Figure 21. Stress Wave After Propagation into Material

Equation (74) has been evaluated by numerical integration to provide a general solution for arbitrary deposition as long as the temperature is given by the adiabatic assumption. In order to see the results of this calculation, the condition was solved for various values of deposition time, 0, and the stress was examined deep into the material as the stress wave passed.

The amplitude of the stress wave was determined as a function of time by picking a time just before any disturbance within 2δ of the surface could arrive

$$t_0 = \frac{Y - 2\delta}{c}$$

and a time which a wave of duration θ would be fully developed

$$t_1 = \frac{-Y}{c} + \theta + \frac{2\delta}{c}$$

and observing the pulse during this interval. Results for stress as a function of time are shown in Figure 22.

It is seen in Figure 22 that for pulse durations of 10^{-10} seconds, the maximum wave amplitude is 3980 psi with a γ of 10 psi/°C. This corresponds to

$$\sigma_{MAX} = \frac{\gamma T_{MAX}}{2}$$

one-half of the maximum possible initial compressive wave amplitude predicted by Eq. (69). At longer pulse durations, this amplitude diminishes, as for the case of $\theta = 3 \times 10^{-9}$ sec, in Figure 22. The ratio of the stress wave amplitude divided by maximum initial compressive wave is given for various values of pulse duration in Figure (23). The stress wave amplitude approaches zero as the pulse gets longer than $\sim 3 \times 10^{-8}$ sec. Notice that a useful criterion for this case is that an approximate measure of the response time is given by

$$t_r \simeq \frac{\text{deposition range}}{\text{velocity}} \sim \frac{2(1 \times 10^{-4})}{10^5} = \underline{2 \times 10^{-9} \text{ sec}}$$

Figure 22

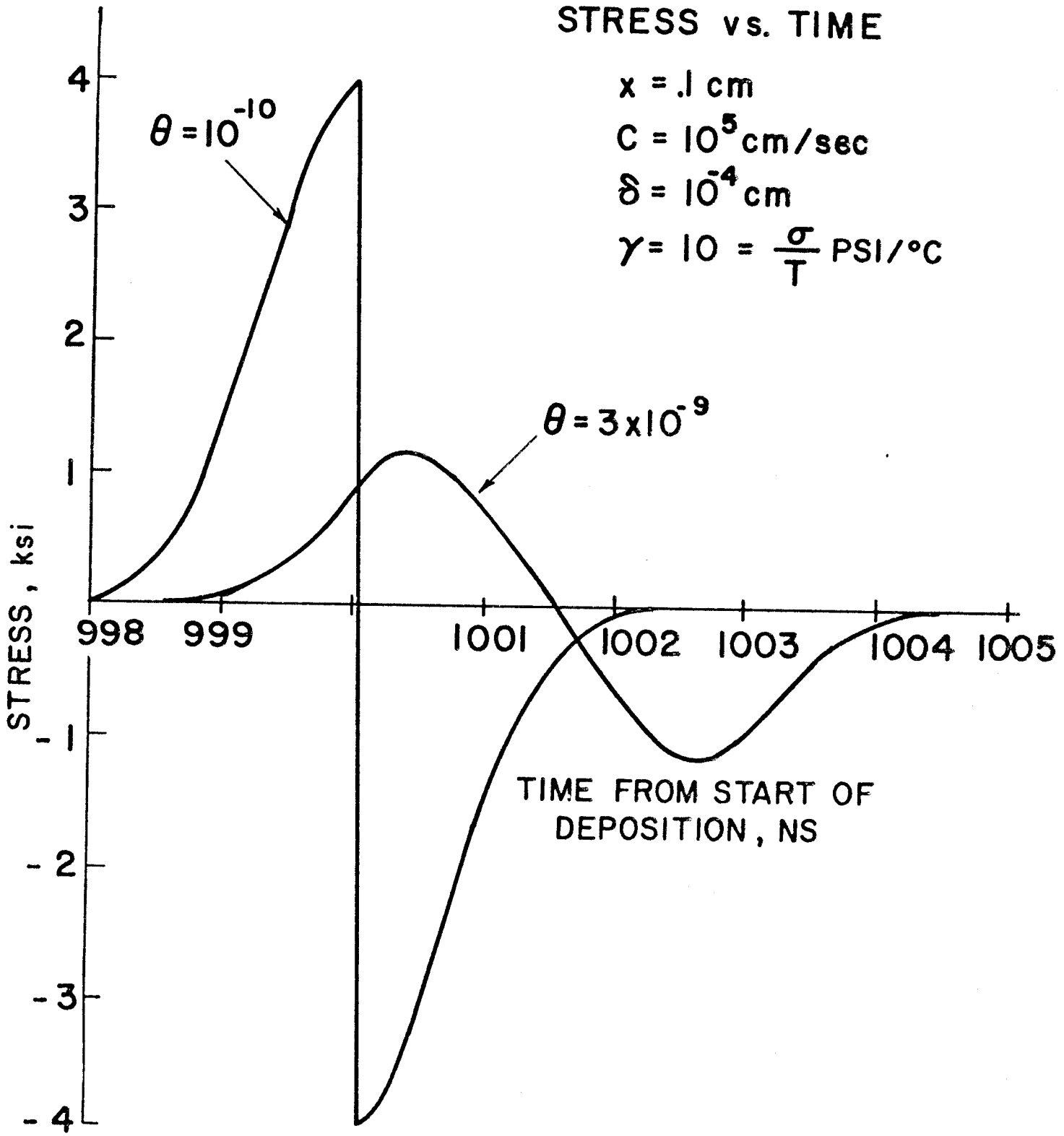
STRESS vs. TIME
x = .1 cm
C = 10^5 cm/sec
δ = 10^-4 cm
γ = 10 = σ/T PSI/°C
θ = 10^-10
θ = 3x10^-9
STRESS, ksi
4
3
2
1
-1
-2
-3
-4
998
999
1001
1002
1003
1004
1005
TIME FROM START OF DEPOSITION, NS

At any time longer than this, the amplitude is reduced as the stress is propagating away faster than it is created. Also shown in Figure 23 is the front surface temperature response from Figure 18 which indicates that for all times of interest for stress wave generation, there is negligible heat conduction. If spatial profiles were chosen with sharper gradients, the relative response times between stress and temperature might be closer.

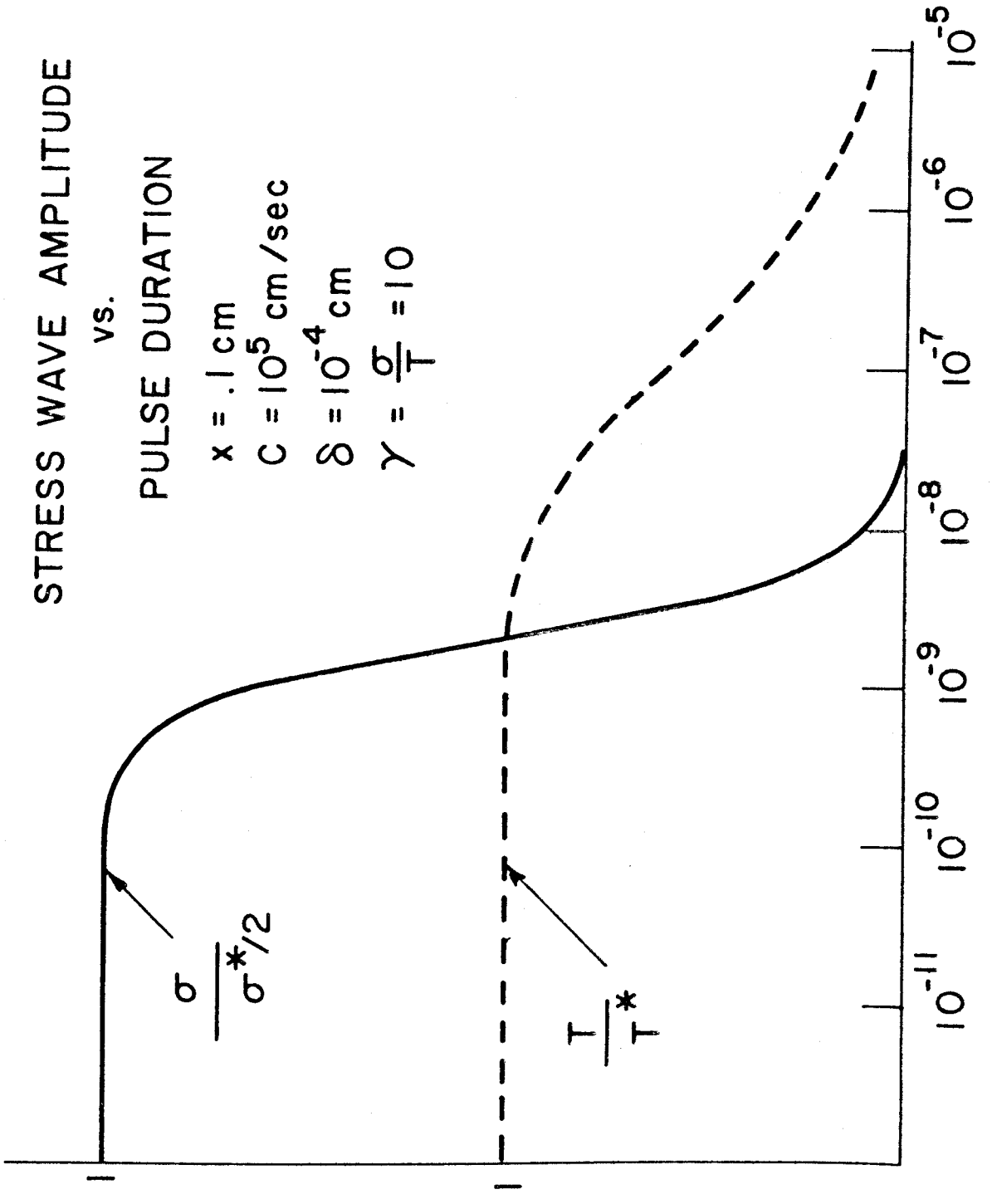
STRESS WAVE AMPLITUDE
vs.
PULSE DURATION
x = .1 cm
C = 10^5 cm/sec
δ = 10^-4 cm
γ = σ̄/T = 10
σ/σ*/2
T/T*
1
1
10^-11
10^-10
10^-9
10^-8
10^-7
10^-6
10^-5
PULSE DURATION, SEC

Figure 23

II-D. Displacement Response

The displacement production from an arbitrary spectrum of charged particles or neutrons can be determined upon specification of the spatial and temporal distributions of the fluxes and the appropriate dpa cross-section. This is conceptually easy for neutrons if the flux, as determined by time dependent neutronics, is multiplied by the cross section for the material in question. For ions, the process is normally more complex, since damage is limited to regions near the exposed surface and distributions for monoenergetic incident ions are determined by ion implantation codes. In the following section, procedures are outlined whereby efficient, yet approximate, calculations can be performed for ions of various energies.

II-D-1. Ions $Z \leq 2$

A model for light ions with energies greater than a few tens of KeV can be developed from the spatial energy distributions which were presented in Section II-A. This formulation allows the ion energy to be specified at any position and is accurate at all points except very near the end of range. Although the nuclear damage is ignored in determining the transport characteristics, it can still be evaluated as a function of ion energy. This damage then becomes the local displacement rate at the position where the energy is specified.

The methodology in this paper is commensurate with that of Doran et al.[14] in a working group report on displacements and procedures for damage calculations. The approach in this study was to extend these procedures to determine energy and spatial dependence.

Upon determination of the mean ion energy as a function of position, it is necessary to develop an appropriate displacement cross section. Two alternative procedures are available:

1) a Binary Rutherford interaction model which accounts for the effective charge of the ion; and
2) the Lindhard (LSS)[4] model based on a Thomas-Fermi potential

The former is consistent with reference 14 and consists of expressing the Rutherford differential scattering cross section as

76) $$d\sigma(E) = \frac{B\gamma^2}{E}\frac{dT}{T^2}$$

where

76a) $$B = \frac{4\pi a_0^2 m_1 z_1^2 z_2^2 E_r^2}{m_2}$$

a_0 = Bohr radius = 0.53 Å

m_1 = ion mass

z_1 = ion atomic number

z_2 = target atomic number

E_r = Rydberg energy = 13.6 ev

m_2 = target mass

T = PKA energy

γ = effective charge given by Bichsel[15] as

76b) $$\gamma = 1 - \exp(-1.316y + 0.1112y^2 - 0.0650y^3)$$

$y = 100B/Z^{2/3}$

$B = v/c$

v = ion velocity

c = velocity of light

Z = ion atomic number

A displacement cross section can be determined from the differential cross section if the number of displacements produced by a PKA of energy T can be established. This is usually accomplished by the selection of an energy partition model and a secondary displacement model.

The energy partition model accounts for the relative distribution of the PKA energy loss between the electrons and nuclei. The latter process is the only one used in determining displacements. A convenient form which approximates the function discussed in LSS theory is given by Robinson[16] as

77) $$T_{damage} = \frac{T}{g(\varepsilon)}$$

where

78) $$g(\varepsilon) = 1 + k\varepsilon + 0.40244k\varepsilon^{3/4} + 3.4008k\varepsilon^{1/6}$$

k = LSS stopping parameter which for PKA s is

$$k = 0.1337\ z^{2/3}/A^{1/2}$$

ε = Lindhard reduced energy = T/E_L

$$E_L = 0.08693\ z^{7/3}$$

The secondary displacement model accounts for the displacements produced in a cascade of a PKA with a specified damage energy. The recommended value in Reference 14 is

79)
$$N_d = 0 \qquad T < E_d$$
$$N_d = 1 \qquad E_d \leq T < 2E_d$$
$$N_d = \frac{0.8}{2E_d} T_{dam} \qquad 2E_d \leq T$$

where E_d is the effective displacement energy. Combining Eqs. (76), (77), and (79), yields the displacement cross section as

80) $$\sigma_d(E) = \frac{B\gamma^2}{E}\left\{\int_{E_d}^{2E_d}\frac{dT}{T^2} + \int_{2E_d}^{T_{MAX}}\frac{0.8}{2E_d}\,T\,\frac{dT}{g(T)}\right\}$$

where

$$T_{MAX} = \Lambda E = \frac{4m_1m_2}{(m_1 + m_2)^2}E$$

Equation (80) can only be easily evaluated by numerical integration, which tends to limit its utility. The difficulty in obtaining a closed form integral is the function g(T). The Rutherford cross section, however, is very small angle (or low energy transfer) biased and the function g(T) is a slowly varying function of T at low energies, hence it is reasonable to assume g(T) is approximately a constant whose value is equal to the function evaluated at the average PKA energy where

$$T_{AVE} = 2E_d\text{Log}(T_{MAX}/2E_d)/(1 - 2E_d/T_{MAX})$$

The range of the function g(T) for protons on nickel is shown in the following data:

E (KeV)		$T_{MIN}(2E_d)$ (KeV)	T_{AVE} (KeV)	T_{MAX} (KeV)
50		.080	.1786	3.294
	g(T) =	1.148	1.169	1.280
100		.080	.2054	6.588
	g(T) =	1.148	1.173	1.318

The data indicate that for a low energy transfer cross section g(T) can be assumed constant with only a few percent error. If this assumption is made, Eq. (80) can be integrated as:

81) $$\sigma_d(E) = \frac{B\gamma^2}{E\,E_d}\left\{0.5 + \frac{0.4}{g(\bar{T})}\,\ell n\,\frac{T_{MAX}}{2E_d}\right\}$$

units = $\mathring{A}^2$, energy = eV

B = Equation (76a)

γ = Equation (76b)

E = ion energy

E_d = displacement energy

T_{MAX} = maximum PKA energy

Results from Eq. (81) were found to yield the same values (within a few percent) as numerically integrated values in Reference 14 for protons on nickel for ion energies of 100 KeV - 2MeV.

An alternative method for determining the displacement damage in terms of dpa cross section is to use the nuclear stopping power derived in LSS theory. This is the basis of the model used in the methods of Brice,[6] Winterbon,[7] and Manning and Mueller.[8] The essential difference between their approach and the modified Rutherford method discussed above is the treatment of electron screening. In the LSS model, the screening is treated explicitly by assuming an interaction potential based on the Thomas-Fermi model. The modified Rutherford model accounts implicitly for screening by allowing the charge of the moving ion be a function of energy. These approaches, although different in concept, tend to accomplish the same thing.

The differential cross section based on the LSS model was given in Part I (Eq. (27)), in terms of the Lindhard tabulated screening function. Winterbon, et al.[17], also give the analytic approximation:

82) $$d\sigma(E) = \frac{\pi a^2}{2} \lambda\, t^{-4/3}[1 + (2\lambda t^{2/3})^{2/3}]^{-3/2} dt$$

where

$\lambda = 1.309$

$t = \varepsilon^2\, T/T_{MAX} = \varepsilon^2 \sin^2\theta/2$

$a = 0.468(z_1^{2/3} + z_2^{2/3})^{-1/2}$ Å

$\varepsilon = E/E_L$

$E_L = \frac{1 + A}{A} \frac{z_1 z_2 e^2}{a}$

$A = m_2/m_1$

T = PKA Energy

E = ion energy

The nuclear energy loss can be derived from Eq. (82) by performing the integral

83) $$\left.\frac{d\varepsilon}{d\rho}\right|_N = \frac{N R_L}{E_L} \int_{\gamma^2}^{\varepsilon^2} \frac{T_m t}{\varepsilon^2} \frac{d\sigma}{dt}\, dt$$

where

$\rho = r/R_L$ = reduced length

$R_L = \frac{(m_1 + m_2)^2}{N\, a^2 4 m_1 m_2}$

N = atomic number density

$\gamma = \varepsilon(T_L/T_M)^{1/2}$

T_L = lower limit of PKA spectra

Oen,[18] et al, give the value for this integral as

$$84) \qquad \left.\frac{d\varepsilon}{d\rho}\right|_N = \frac{9}{8\varepsilon} \ln\left[\frac{(2\lambda)^{1/3}\varepsilon^{4/9} + (1 + (2\lambda)^{2/3}\varepsilon^{8/9})^{1/2}}{(2\lambda)^{1/3}\gamma^{4/9} + (1 + (2\lambda)^{2/3}\gamma^{8/9})^{1/2}} + \frac{(2\lambda)^{1/3}\gamma^{4/9}}{(1 + (2\lambda)^{2/3}\gamma^{8/9})^{1/2}} - \frac{(2\lambda)^{1/3}\varepsilon^{4/9}}{(1 + (2\lambda)^{2/3}\varepsilon^{8/9})^{1/2}}\right]$$

In order to evaluate a dpa cross section, the following integral must be performed:

$$85) \qquad \sigma(E) = \int_{E_d}^{2E_d} \frac{d\sigma}{dT}\, dT + \int_{2E_d}^{T_M} \frac{d\sigma}{dT} \frac{0.8T\, dT}{2E_d\, g(T)}$$

Again, if g(T) is approximately constant, this can be transformed into

$$86) \qquad \sigma(E) = \int_{E_d}^{2E_d} \frac{d\sigma}{dT}\, dT + \frac{E_L}{NR_L}\left[\frac{0.4}{E_d\, g(T)}\right] \left.\frac{d\varepsilon}{d\rho}\right|_N$$

where the term $\left.\frac{d\varepsilon}{d\rho}\right|_N$ is [Eq. (84)] evaluated for ε and $\gamma = (2E_d/T_m)^{1/2}$. The first integral in Eq. (85) can be estimated by

$$\frac{d\sigma}{dt}(t_0)\Delta t$$

where

$$\Delta t = \varepsilon^2\, E_d/T_m$$

$$t_0 = \varepsilon^2\, 3E_d/2T_m$$

$$\frac{d\sigma}{dt} = \text{Equation (82)}$$

An estimate of the dpa cross section for light ions can, at this point, be derived from Eq. (81) (modified Rutherford) or Eq. (86) (LSS, Thomas-Fermi). A comparison of these two values for protons on copper is shown in Figure 24. In this case, the energy partition function was assumed to be unity for both cases. It is noted that small differences are noted at higher energies (100 KeV and up) but differences of a factor of 5 or more are evident in the few KeV regions. In this study, the LSS value was used so that results could be compared with the ion implantation codes which use the same formulation. A more rigorous approach to resolve the discrepancies evident at low energies would be to use alternate potential functions in such codes. The methods in this study are approximate and are most accurate at higher energies where the disagreement is negligible.

The procedure for evaluating the local displacement rate for light ions would be as follows:

87) $$\dot{D}(x,t) = f(t)\sigma_{dpa}[E(x,E^*)]$$

where $f(t)$ is the instantaneous flux of ions of energy E^* at the exposed surface.

$E(x,E^*)$ is the energy of an ion of incident energy E^* at position x (Table I).

$\sigma_{dpa}(E)$ is the dpa cross section for an ion of energy E in the target (Eq. (81) or (86)).

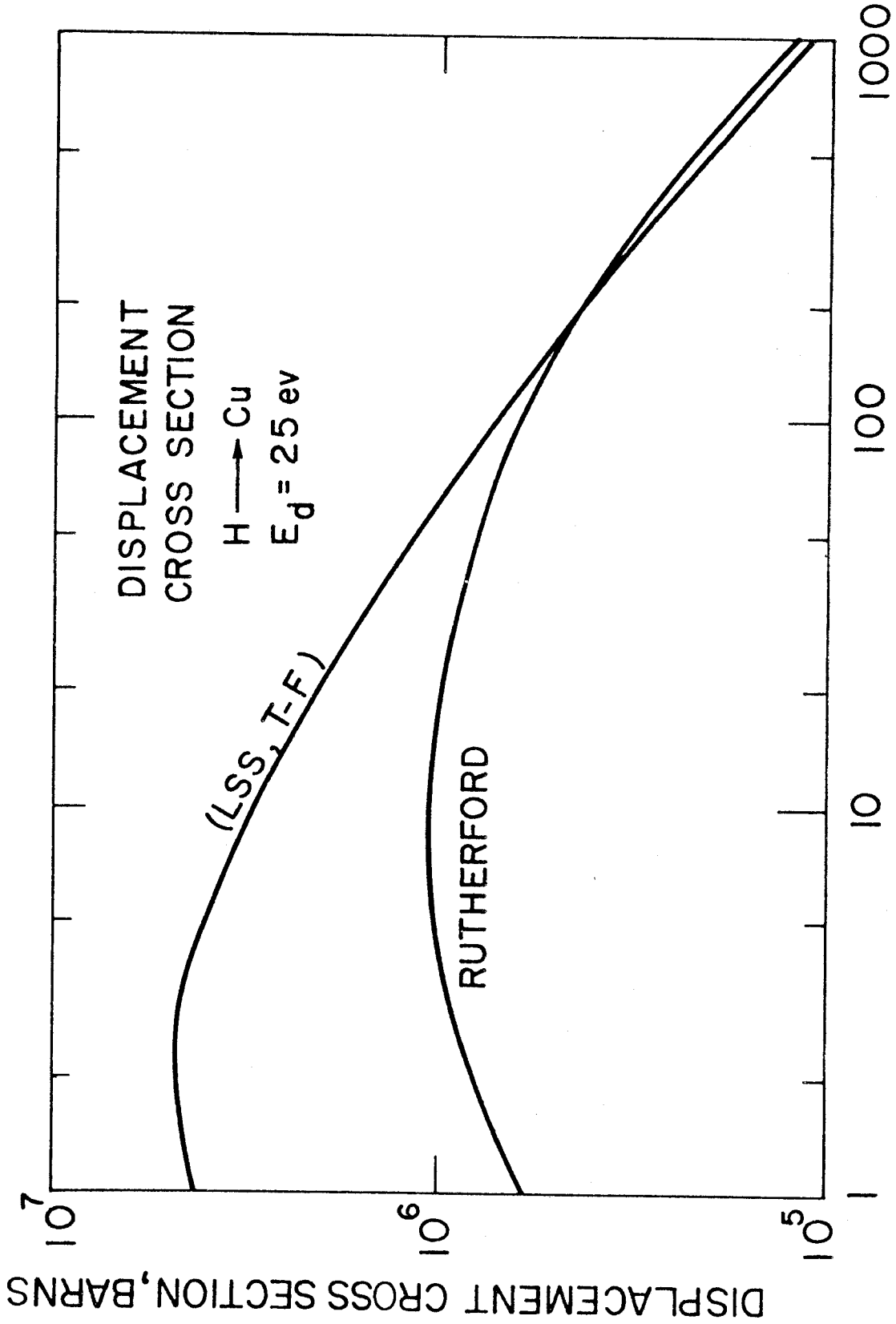
DISPLACEMENT CROSS SECTION, BARNS
ENERGY, KeV
DISPLACEMENT CROSS SECTION
H ⟶ Cu
E_d = 25 ev
(LSS, T-F)
RUTHERFORD
10^7
10^6
10^5
1
10
100
1000

Figure 24

II-D-2. Displacements for Ions of Z > 2

For heavier ions, the determination of local displacement production is more complex, because the mean energy of an ion is not so easily determined, and the effects of scattering and straggling are more pronounced. One must, therefore, rely on one of the ion implantation codes. If various spectra of ions are to be studied, however, it is necessary to develop a technique to determine the spatial displacement profiles in a more efficient form.

This requirement is in part due to the considerable expense associated with multiple runs of the ion codes.

The technique developed in this study involves the definition of a new form of the dpa cross section (or damage factor) as:

$$\sigma^{*}_{dpa} = \sigma^{*}_{dpa}(E^{*},x) \tag{88}$$

In this case, the cross section contains information on both the amplitude and spatial extent of the displacement of an ion of incident energy E*. These damage factors can be used to calculate the damage at any position as simply as:

$$\dot{D}(x,t) = f(t)\sigma^{*}_{dpa}(E^{*},x) \tag{89}$$

These damage factors are determined by performing a single set of ion implantation calculations (as with the Brice codes RASE 4 and DAMG 2 in this study) at selected ion energies covering all potential spectra of interest. The results of these calculations are then parameterized by determining a numerical fitting function or a set of functions whose defining coefficients can be expressed as functions of energy. An example of the damage distribution from which the damage factors can be determined is shown in Figure 25. These data are for aluminum ions onto nickel, although similar data were employed for other ion-target combinations.

Figure 25

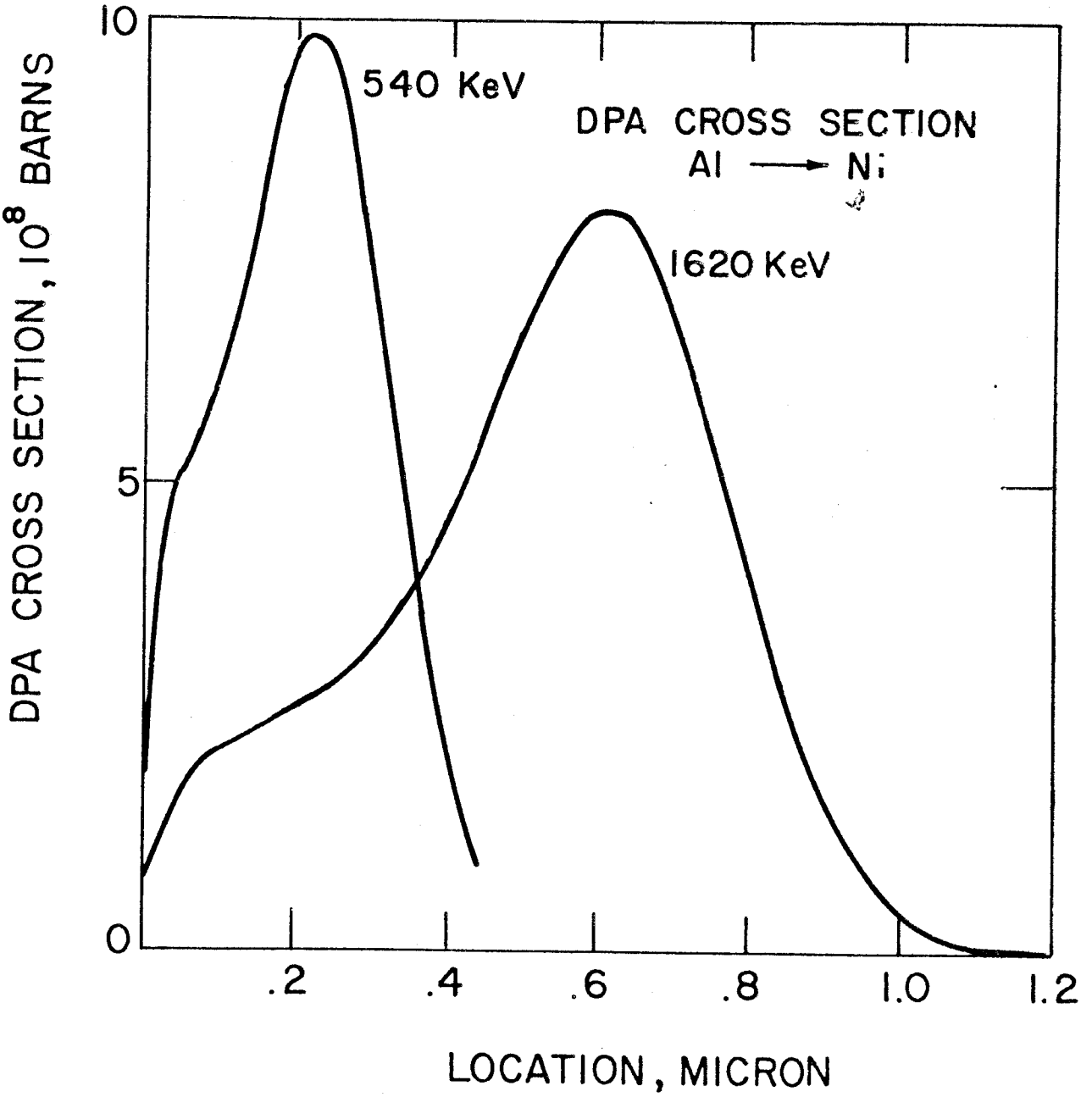
10
5
0
DPA CROSS SECTION, 10^8 BARNS
540 KeV
DPA CROSS SECTION
Al → Ni
1620 KeV
.2
.4
.6
.8
1.0
1.2
LOCATION, MICRON

III. Application to Specific Pulsed Fusion Spectra

The models discussed in Chapter II allow determination of the temperature, stress and displacement production at any location in a material exposed to particular set of radiation spectra. In this chapter a brief example of this application of these models to specific spectra and materials is given. Examples are more fully discussed in reference 19 and a detailed examination of the utility of these models is planned for Part III in this same series.

The reference spectra chosen for this example are similar to bare pellet spectra from laser fusion systems. The components of this spectra are given in Table IV. In this case an additional component, Si, was added to the pellet debris to indicate the effect of heavy ions on the temperature and displacement response. The material chosen for this example was copper at a distance of 7 meters.

The front surface energy deposition is shown in Figure 26 while the total energy deposition profiles for each ion component is shown in Figure 27 at the end of each respective pulse.

The temperature excursion above ambient at the front surface for each component is shown in Figure 28. In this case the X-ray response was determined from an impulse source assumption while the laser light was deposited over a period of 10 ns. The total temperature response is shown in Figure 29 at the front surface, and at positions 1 and 5 microns from the exposed surface.

Table IV

Reference Spectra (100 MJ)

	Energy (MJ)	Spectrum
Laser	.2	10.6 μ
X-Ray	2	1.0 keV - BB
D	4.6	160 keV - M
T	6.9	240 keV - M
He (Slow)	1.2	320 keV - M
He (Fast)	5.4	2 ± .5 MeV - G
Silicon	2.7	800 keV - M
Neutrons	77.	14 ± 1 MeV - G

BB = Black Body M = Maxwellian G = Gaussian

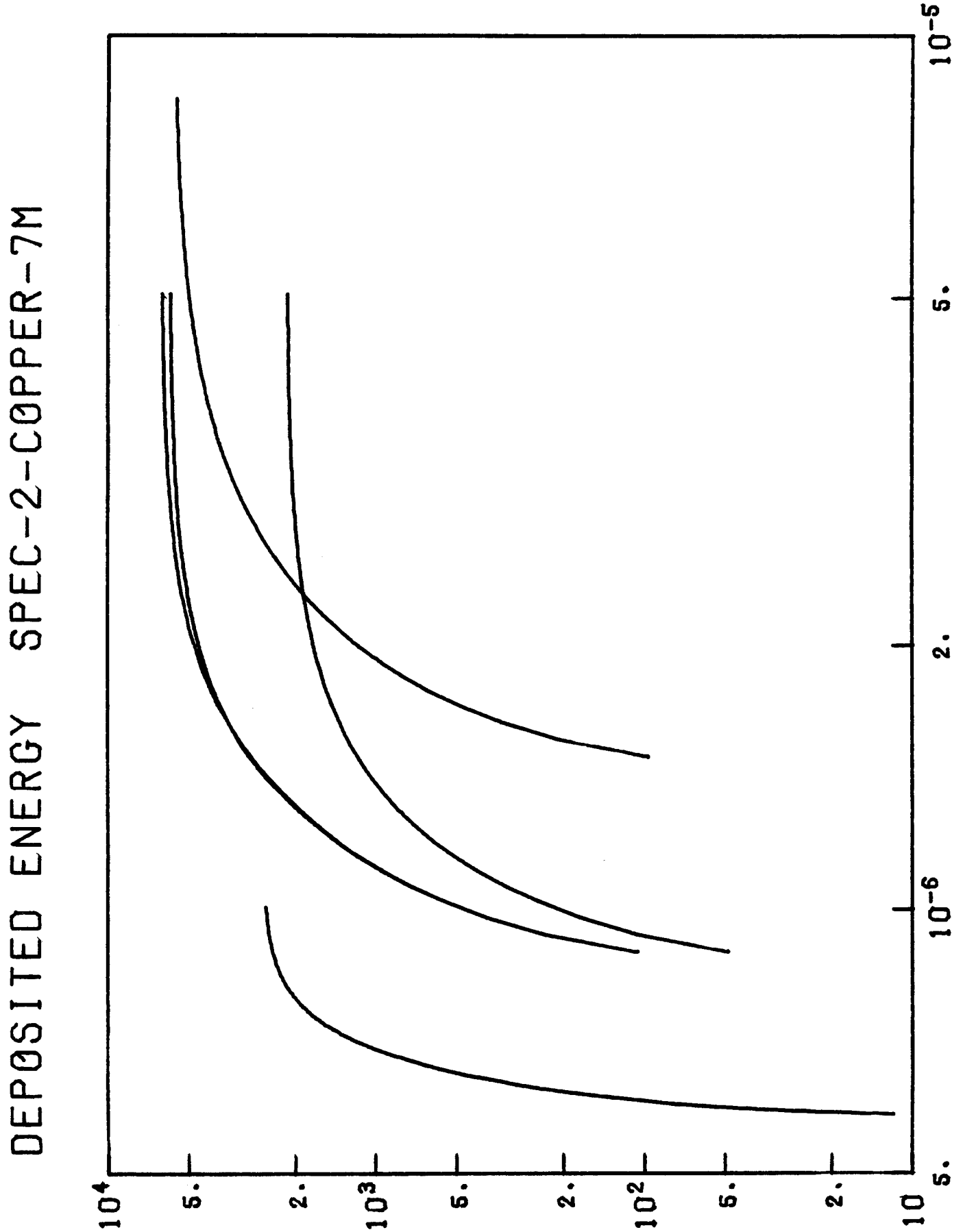
DEPOSITED ENERGY SPEC-2-COPPER-7M
JOULES/CM3
TIME,SEC
10^4
5.
2.
10^3
5.
2.
10^2
5.
2.
10
5.
10^-6
2.
5.
10^-5

Figure 26

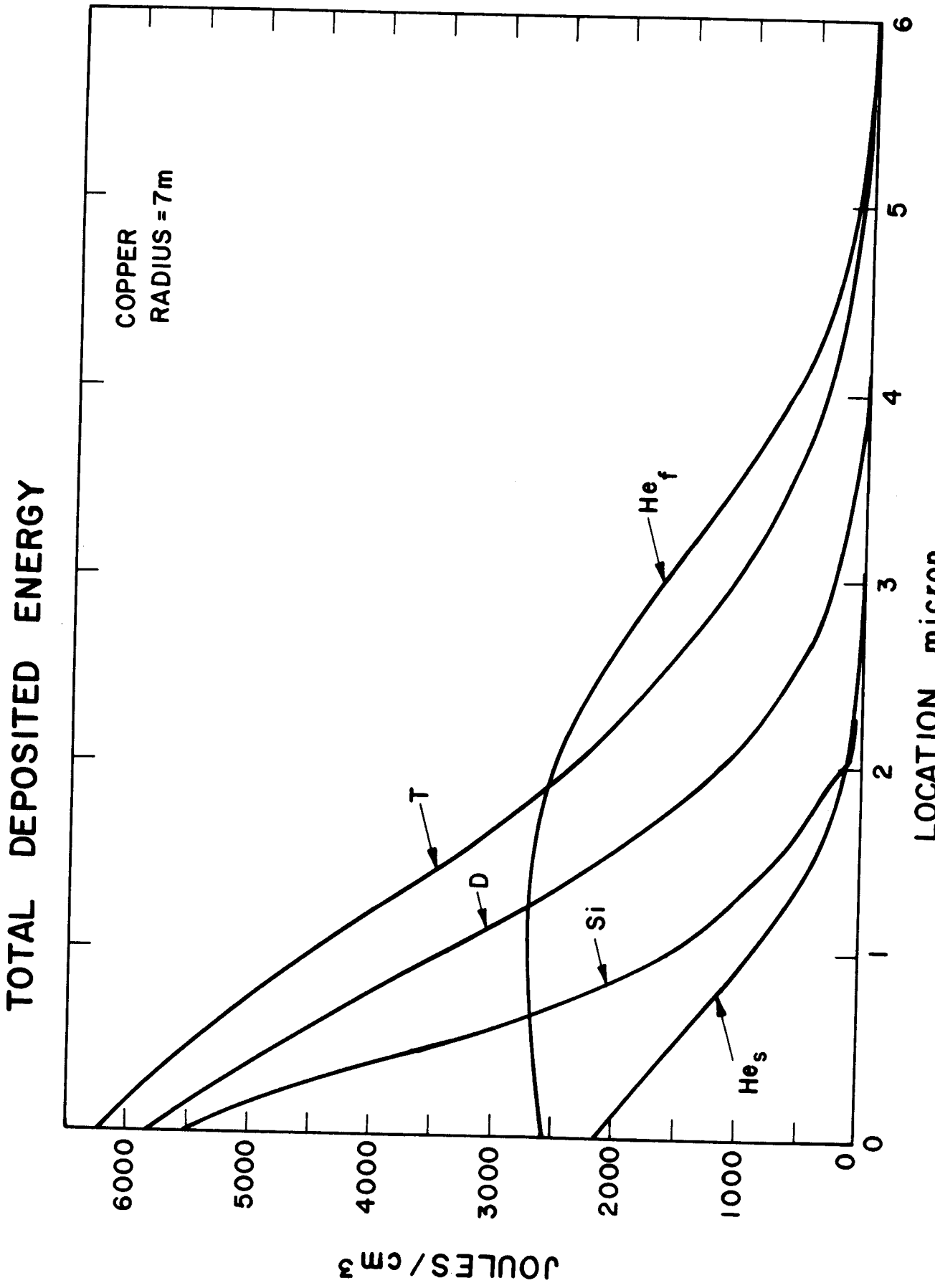
TOTAL DEPOSITED ENERGY
COPPER
RADIUS = 7m
JOULES/cm³
LOCATION , micron
T
D
Si
He_f
He_s
0
1000
2000
3000
4000
5000
6000
0
1
2
3
4
5
6

Figure 27

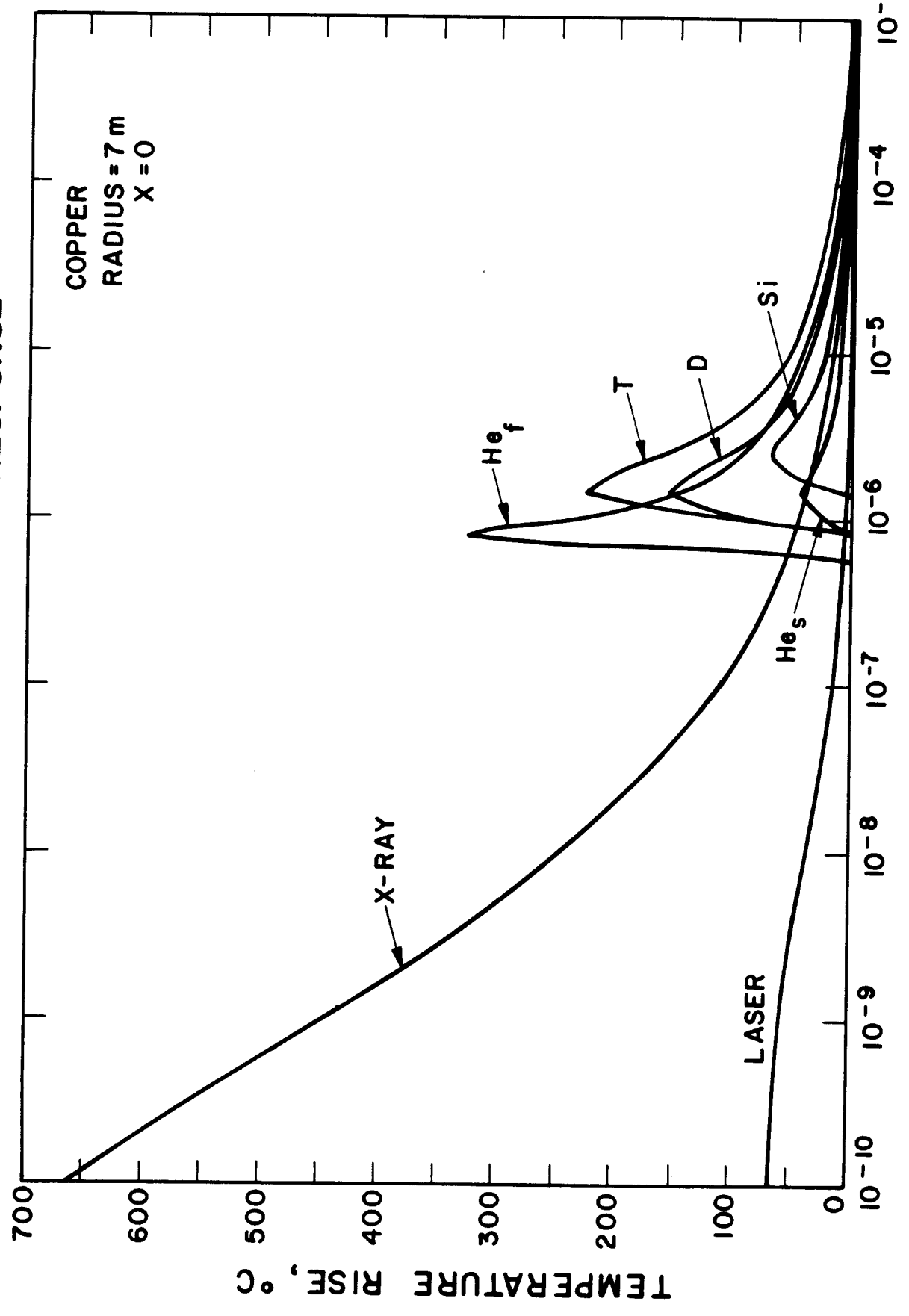
COMPONENT TEMPERATURE RESPONSE
COPPER
RADIUS = 7 m
X = 0
X-RAY
LASER
He_f
T
D
Si
He_s
TEMPERATURE RISE, °C
TIME AFTER X-RAY ARRIVAL, sec.
700
600
500
400
300
200
100
0
10^{-10}
10^{-9}
10^{-8}
10^{-7}
10^{-6}
10^{-5}
10^{-4}
10^{-3}

Figure 28

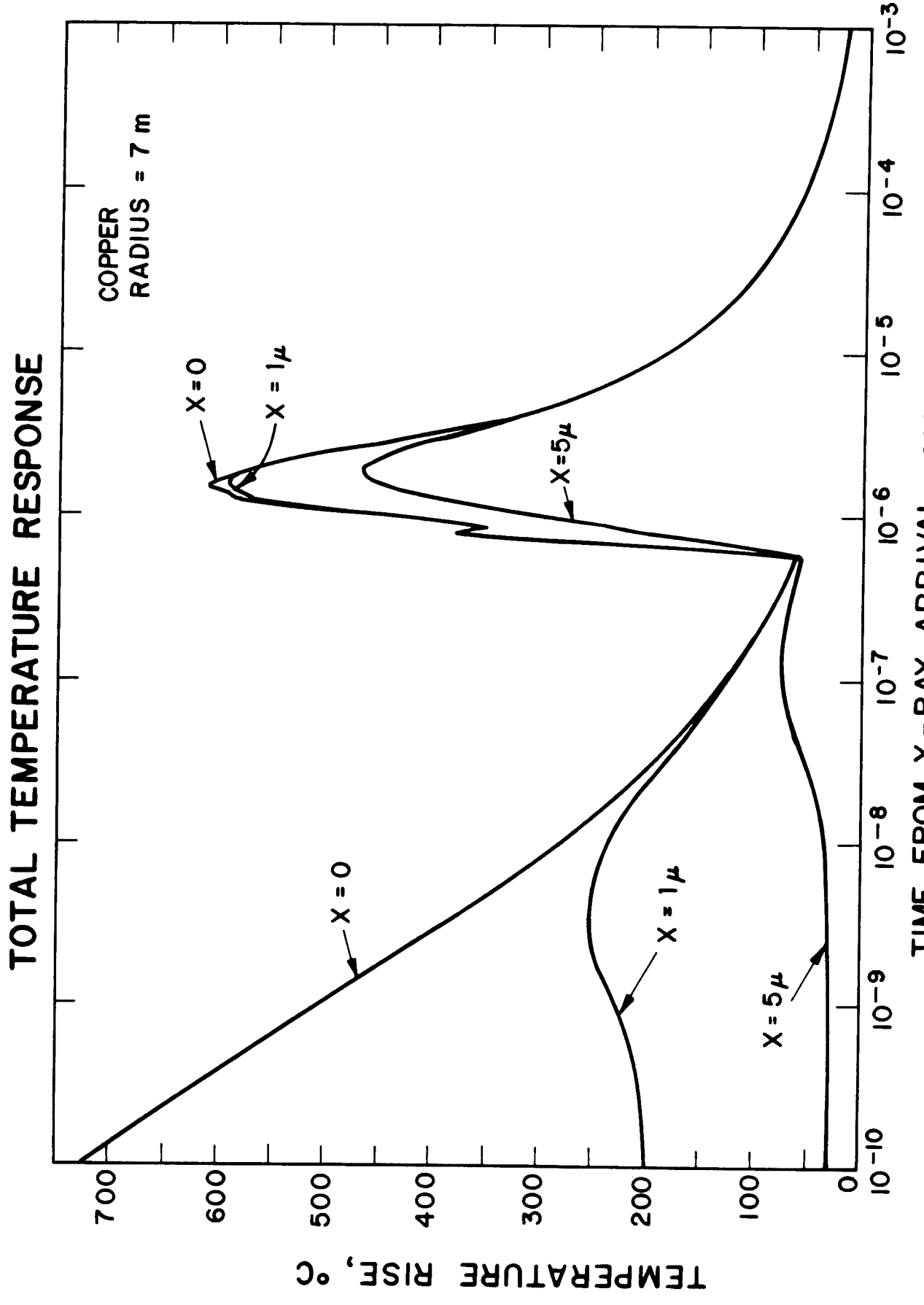
TOTAL TEMPERATURE RESPONSE
COPPER
RADIUS = 7 m
X=0
X = 1μ
X=5μ
X = 0
X = 1μ
X = 5μ
TEMPERATURE RISE, °C
TIME FROM X-RAY ARRIVAL, sec.
700
600
500
400
300
200
100
0
10⁻¹⁰
10⁻⁹
10⁻⁸
10⁻⁷
10⁻⁶
10⁻⁵
10⁻⁴
10⁻³

Figure 29

The displacement rate from each component is shown in Figure 30 for the front surface and in Figure 31 at 1 micron. All components exhibit higher displacement cross section as their energy is reduced near the end of range. The total displacement rate at the front surface and at 1 micron is shown in Figure 32. The superposition of the total temperature and displacement rate at both positions is shown in Figures 33 and 34.

The synergism of the transient temperature and displacement production will significantly affect the various responses of the materials to pulsed fusion sources. The role of these effects on sputtering, blistering and clustered defects will be discussed in subsequent sections of this series.

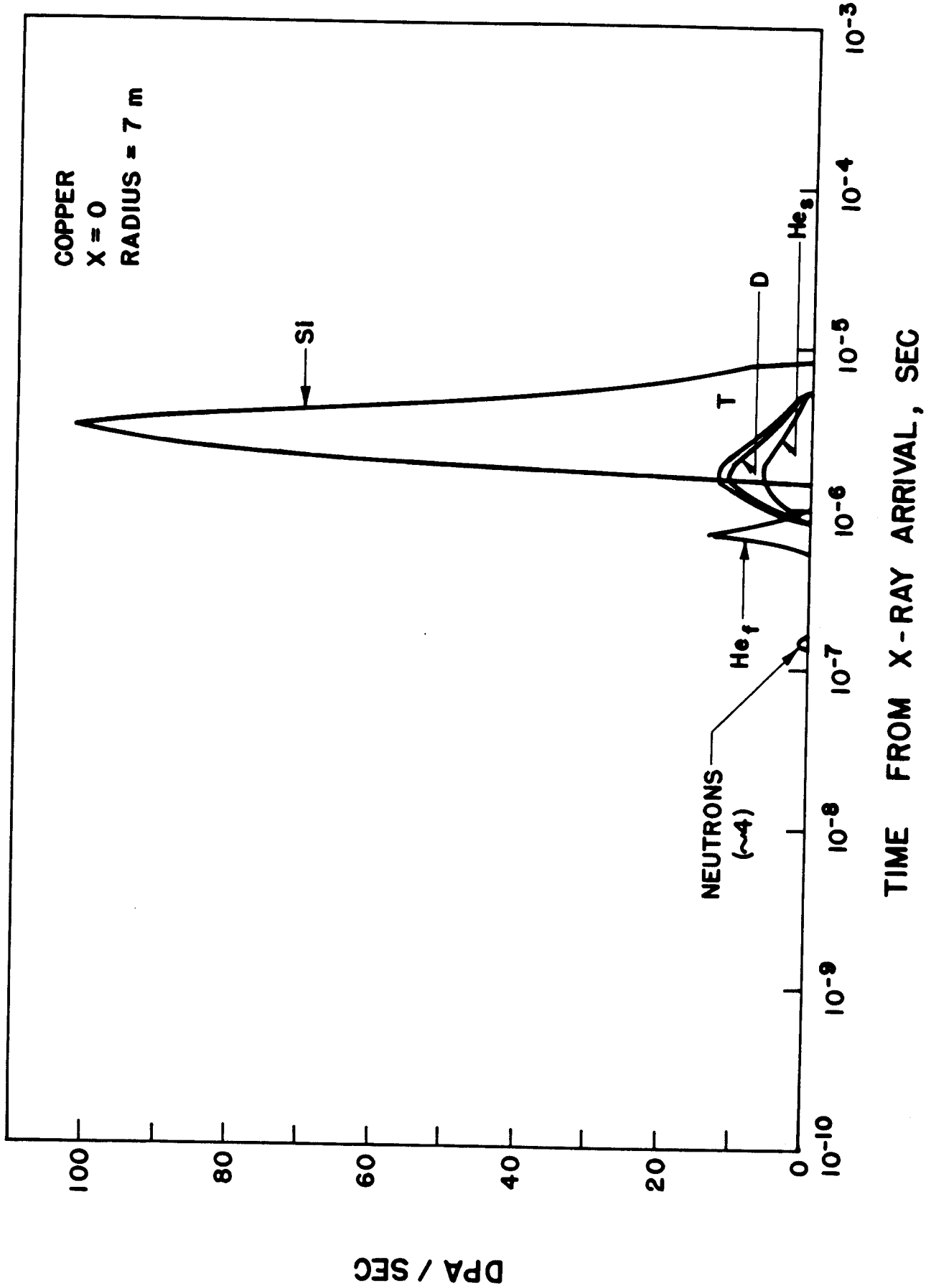
COMPONENT DISPLACEMENT RATE
COPPER
X = 0
RADIUS = 7 m
Si
T
D
He_s
He_f
NEUTRONS
(~4)
DPA / SEC
TIME FROM X-RAY ARRIVAL, SEC
0
20
40
60
80
100
10^{-10}
10^{-9}
10^{-8}
10^{-7}
10^{-6}
10^{-5}
10^{-4}
10^{-3}

Figure 30

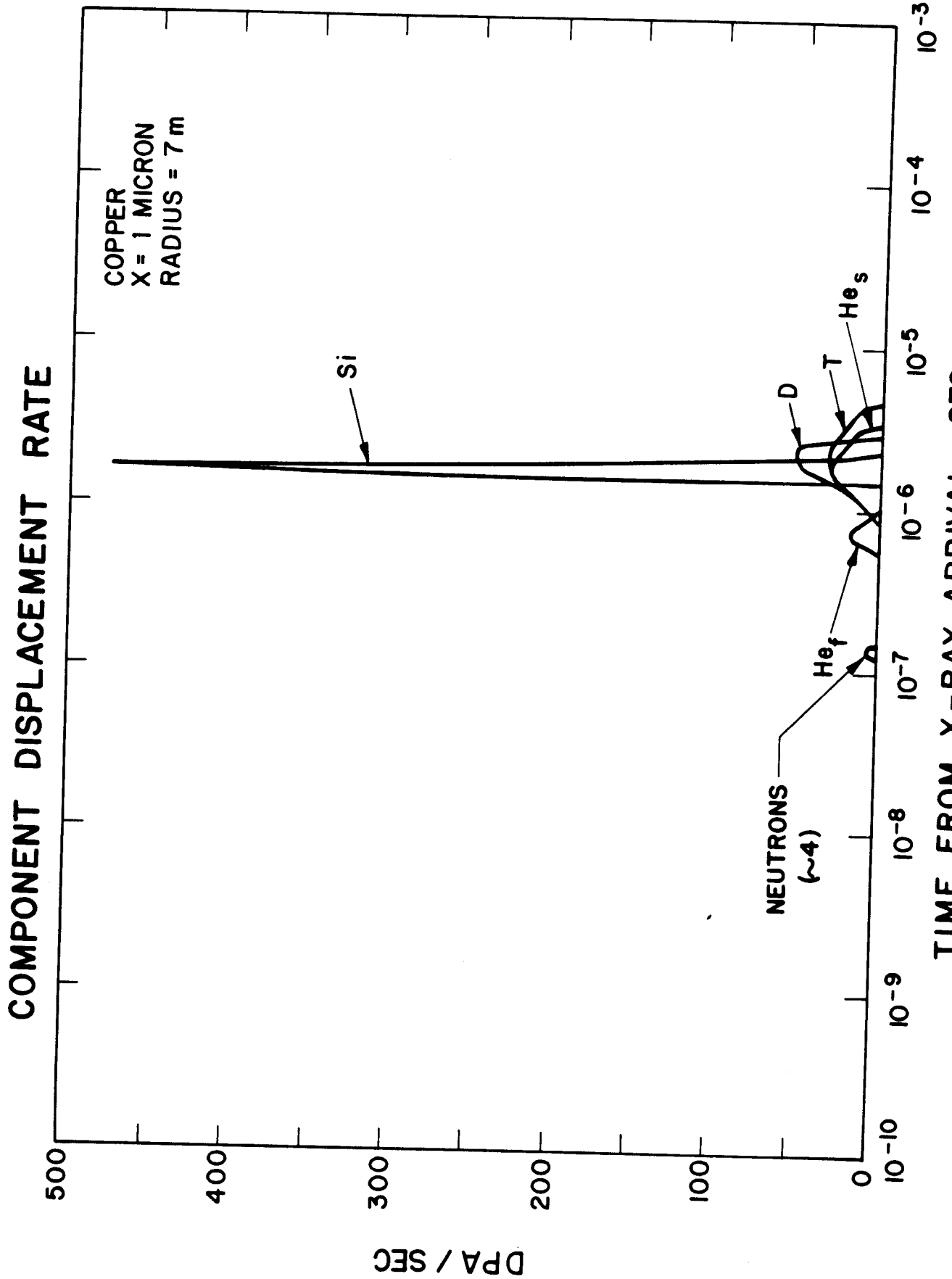
COMPONENT DISPLACEMENT RATE
COPPER
X = 1 MICRON
RADIUS = 7 m
Si
D
T
He_s
He_f
NEUTRONS
(~4)
DPA / SEC
TIME FROM X-RAY ARRIVAL, SEC
500
400
300
200
100
0
10^-10
10^-9
10^-8
10^-7
10^-6
10^-5
10^-4
10^-3

Figure 31

Figure 32

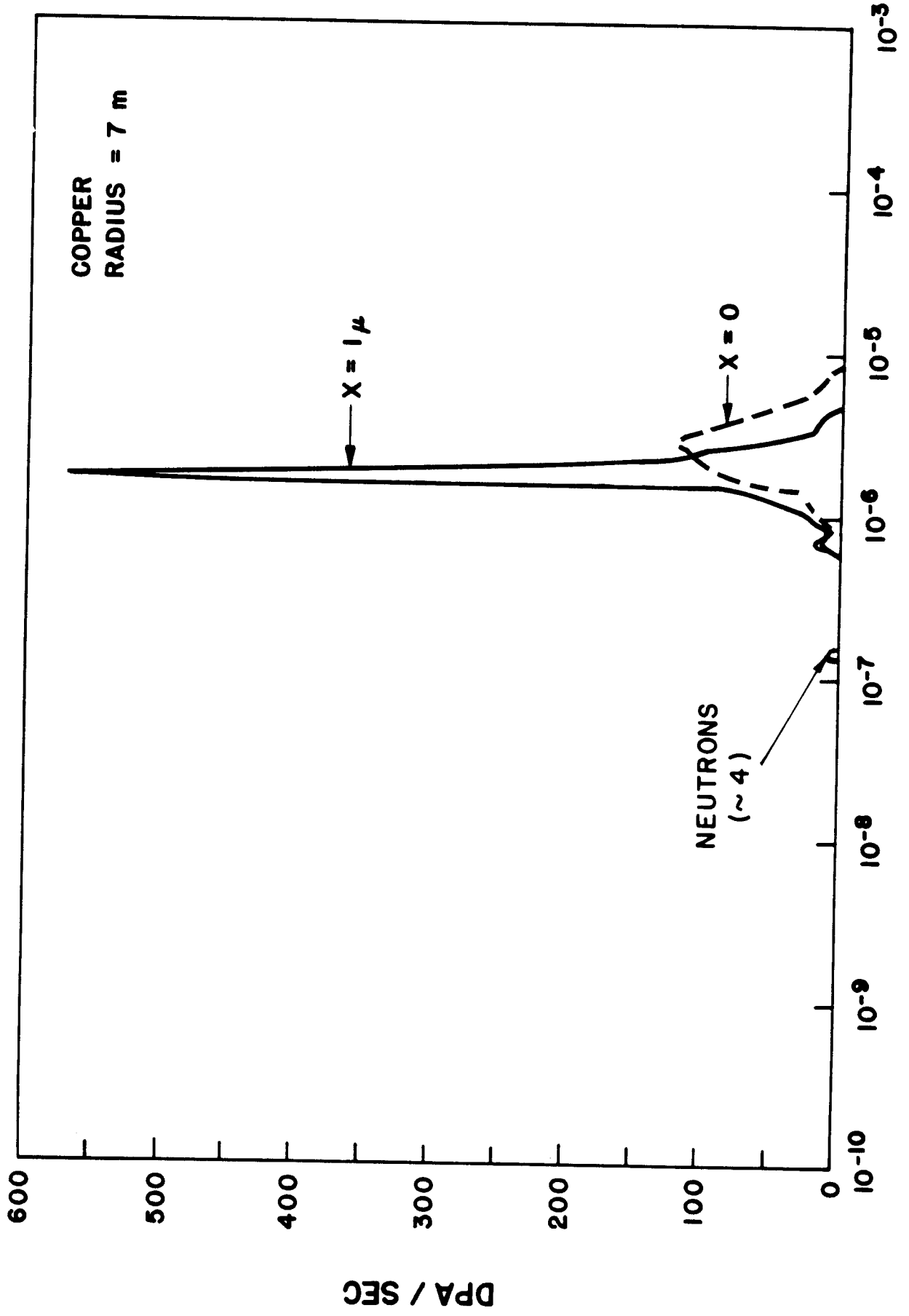
TOTAL DISPLACEMENT RATE
COPPER
RADIUS = 7 m
X = 1 μ
X = 0
NEUTRONS
(~4)
DPA / SEC
600
500
400
300
200
100
0
10-10
10-9
10-8
10-7
10-6
10-5
10-4
10-3
TIME, FROM X-RAY ARRIVAL, SEC

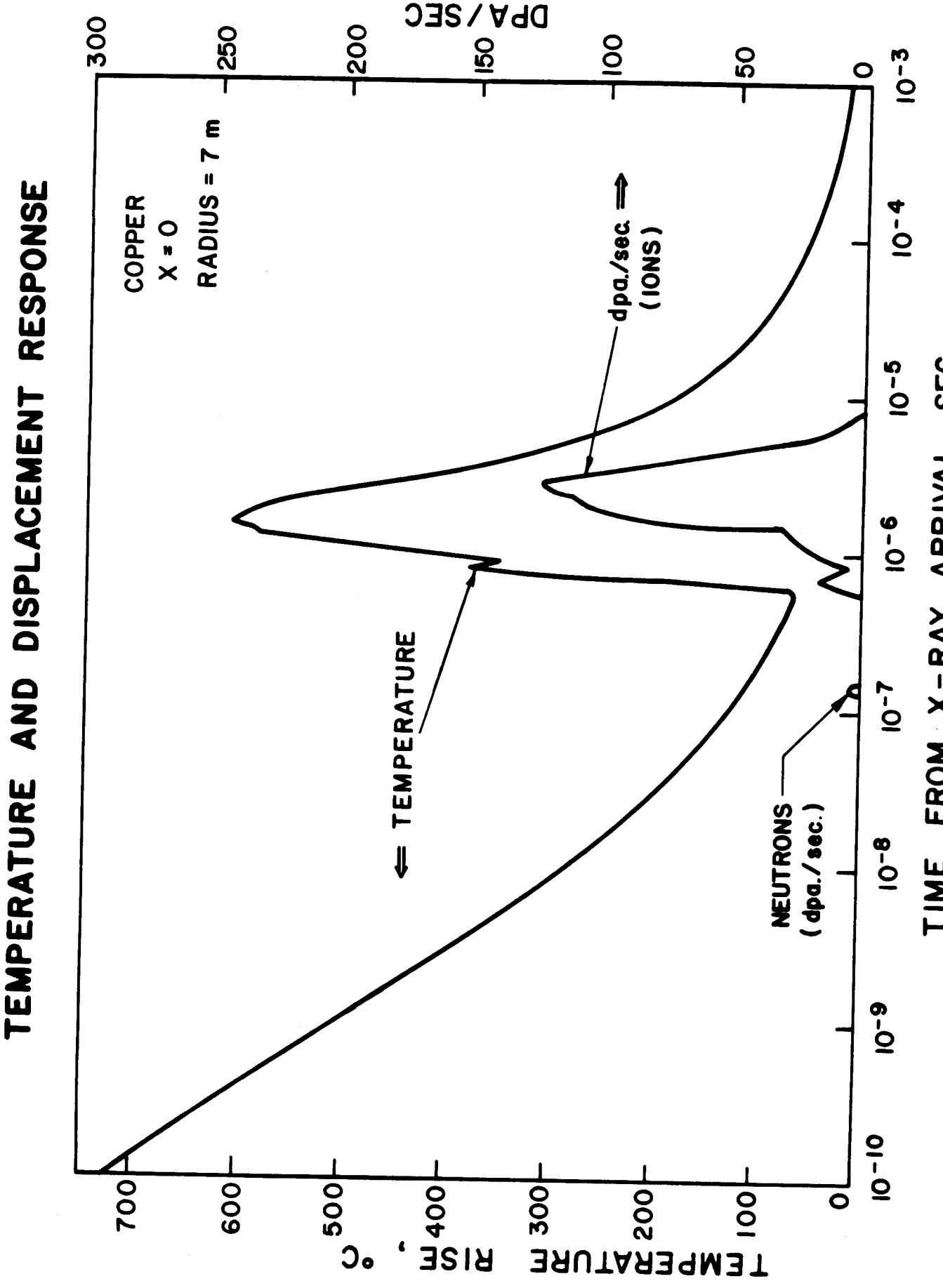
TEMPERATURE AND DISPLACEMENT RESPONSE
COPPER
X = 0
RADIUS = 7 m
dpa./sec ⟹
(IONS)
⟸ TEMPERATURE
NEUTRONS
(dpa./sec.)
TEMPERATURE RISE, °C
DPA/SEC
TIME FROM X-RAY ARRIVAL, SEC
0
100
200
300
400
500
600
700
0
50
100
150
200
250
300
10-10
10-9
10-8
10-7
10-6
10-5
10-4
10-3

Figure 33

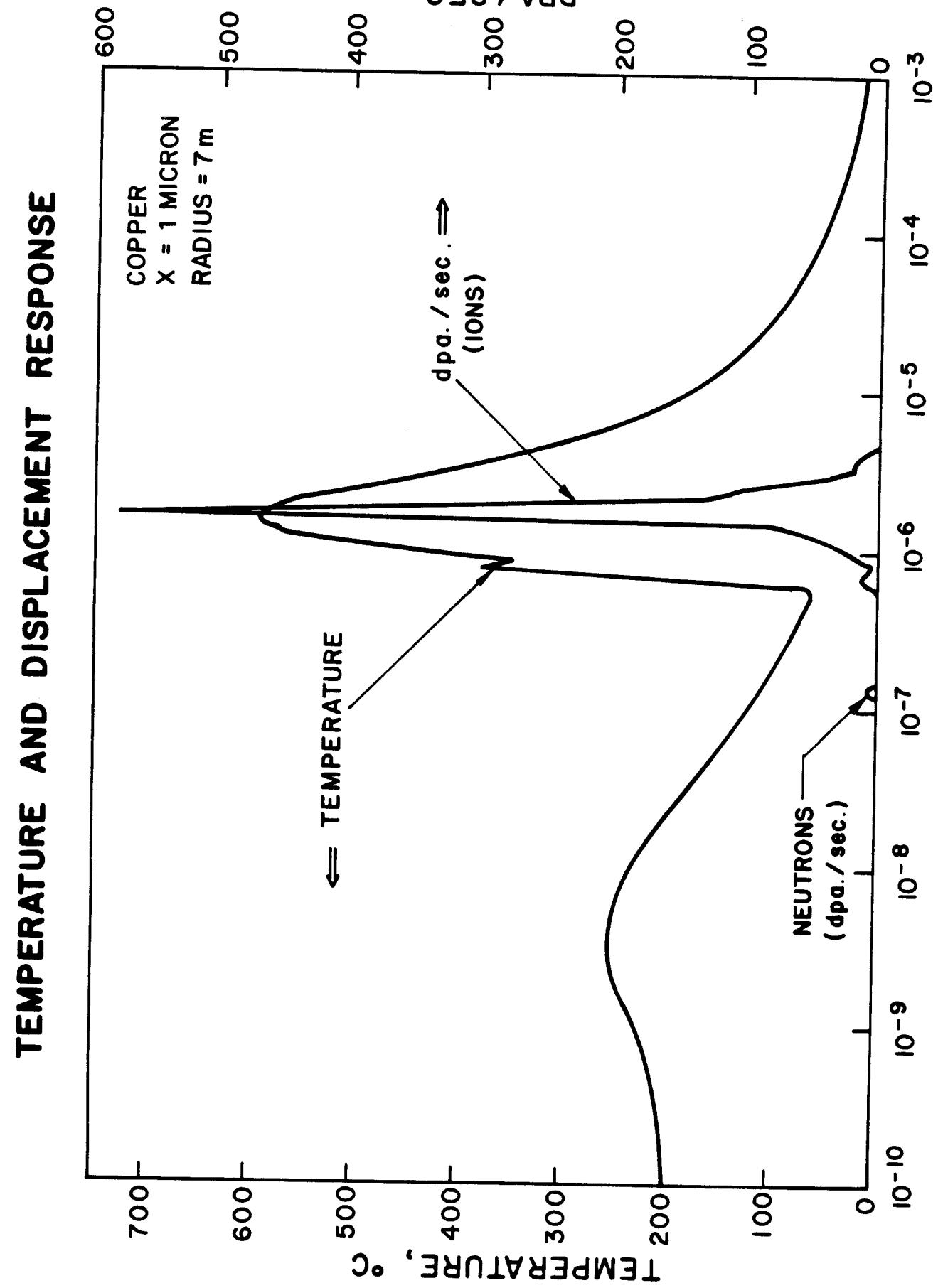
TEMPERATURE AND DISPLACEMENT RESPONSE
COPPER
X = 1 MICRON
RADIUS = 7 m
dpa. / sec. ⟹
(IONS)
⟸ TEMPERATURE
NEUTRONS
(dpa. / sec.)
TEMPERATURE, °C
DPA / SEC
TIME FROM X-RAY ARRIVAL, SEC
700
600
500
400
300
200
100
0
600
500
400
300
200
100
0
10-10
10-9
10-8
10-7
10-6
10-5
10-4
10-3

Figure 34

References

1. Hunter, T. O., and Kulcinski, G. L.; Description of the Response of Reactor First Walls to Pulsed Thermonuclear Radiation (Part I); UWFDM-196, Nuc. Eng. Dept. University of Wisconsin, March 1977.

2. Biggs, Frank; Lighthill, Ruth; Analytical Approximations for X-Ray Cross Sections II, SC-PR-71 0507, Sandia Labs., Albuquerque, N. M., Dec. 1971.

3. The Atomic Nucleus; Evans, R. E.; McGraw-Hill, 1955. pp. 672-745.

4. Lindhard, J., et al,; Range Concepts and Heavy Ion Ranges; Mat. Fys. Medd. Dan. Vid. Selsk, 33, No. 14 (1963).

5. Brice, David K.; Three-Parameter Formula for the Electronic Stopping Cross Section at Non-realivistic Velocities, Vol. 6, No. 5, Physical Review A, November 1972.

6. Ion Implantation Range and Energy Deposition Distributions, Vol. 1, Brice, D. K.,: IFI/Plenum, New York.

7. Ion Implantation Range and Energy Deposition Distributions, Vol. 2., K. B. Winterbon IFI/Plenum, New York.

8. Manning, I and Mueller, G. P.; Depth Distribution of Energy Deposition by Ion Bombardment, Computer Physics Communication, 6, 1973.

9. Brice, D. K.; Ion Implantation Range and Energy Deposition Codes COREL, RASE 4, AND DAMG2, SAND75-0622, Sandia Laboratories, Albuquerque, New Mexico, July 1977.

10. Conduction of Heat in Solids; Carslaw, H. S. and Jaeger, J.C.; 2nd Ed., Oxford, 1959.

11. Handbook of Mathematical Functions, U.S. Dept. of Commerce AMS 55, M. Abramouritz and I. A. Stegon, editors, June 1964.

12. Korn, G. A. and Korn, T. M.; Mathematical Handbook for Scientists and Engineers, McGraw-Hill, 1961.

13. Zaker, T.A; Stress Waves Generated by Heat Addition in an Elastic Solid; Journal of Applied Mechanics, 32, 143, March 1965.

14. Doran, D. G., et al.; Report of the Working Group on Displacement Models and Procedures for Damage Calculations, HEDL-TME 73-76, Hanford Engineering Development Laboratory, December 1973.

15. Bichsel, H.; "Passage of Charged Particles Through Matter", American Institute of Physics Handbook, 3rd Ed. p. 8-142, 1972.

16. Radiation-Induced Voids in Metals, Corbett, J. W., and Ianniello, L. C., eds., National Technical Information Service, CONF-710601, p. 397, April 1972.

17. Winterbon, K. B.; Sigmond, P.; and Sanders, J. B.; Spatial Distribution of Energy Deposited by Atomic Particles in Elastic Collisions, Kgl. Danske Videnskab, Selscab, Mat-Jup. Medd. 37, No. 14 (1970).

18. Oen, O. S., et al.; Ion Radiation Damage, In Applications of Ion Beam to Metals, ed. by S. T. Picraux, E. P., p. 641-650, 1974.

19. Hunter, T. O., Abdel-Khalik, S. I.; Kulcinski, G. L.; Response of First Walls in Inertial Confinement Reactors to Thermonuclear Radiation, UWFDM-221, Nuc. Eng. Dept., University of Wisconsin, October 1977

APPENDIX A

RIGOROUS SOLUTION OF THE INHOMOGENEOUS WAVE EQUATION

Equation (74) was derived in a semi-intuitive fashion but will now be derived in a more formal manner which yields the same result.

The solution to the inhomogeneous wave equation can be found from the theory of Green's function as: ($\sigma = \psi$ in our case)

$$1) \qquad \psi(r,t) = \int_0^t dt \int dV\, G(r,t|r',r')q(r',t') + \int_0^t dt_0 \int dS_0(G\nabla\psi - \psi\nabla G) - \frac{1}{c^2}\int dV_0\left[\left(\frac{\partial G}{\partial t'}\right)_{t'=0}\psi_0(r_0) - G\,\frac{\partial\psi}{\partial t}_{t'=0}\right]$$

where the first integral is the response to the forcing function, the second vanishes for a stress free surface and is assumed to go to zero at infinity. The third accounts for the initial condition.

In one dimension, the Green's function is given by Morse and Feshbach[1]

$$2) \qquad G(x - x',t - t') = -\frac{c}{2}\left[1 - H\left(\frac{|x - x'|}{c} - (t - t')\right)\right]$$

where H is the unit step.

We will now consider two problems:

1. Proof that the response to a single impulse of heat is that given by Eq. (71) or (72) if $q(t,x)$ is given by

$$q(x) = \delta(t)g(x)$$

then

4) $$\frac{\partial T}{\partial t} = \frac{\delta(t)}{\rho c}\, g(x)$$

5) $$\frac{\partial^2 T}{\partial t} = \delta'(t)g(x)$$

Equation (1) gives (with stress free initial conditions):

6) $$\sigma(x,t) = \int_{t'} dt' \int_{x} dx' \frac{c}{2}\left[1 - H\left(\frac{|x - x'|}{c} - (t - t')\right]\delta'(t - t')g(x')\right.$$

for $x' < x$

7) $$\sigma(x,t) = \int_{t'} dt' \int_{x} dx' \frac{c}{2}\left[1 - H\left(\frac{(x - x')}{c} - t - t'\right)\right]\delta'(t - t')g(x')$$

since

8) $$\int_a^b f(x)\delta'(x)dx = \begin{cases} -f'(0) & x = 0 \quad \text{in } a \to b \\ 0 & x = 0 \quad \text{out } a \to b \end{cases}$$

9) $$\sigma(x,t) = \int_{t'} dt' \int_{x} dx' \left\{\frac{c}{2} - \left(\frac{x - x'}{c} - \delta(t - t')g(x')\right\}\right. = \frac{1}{2}\, g(x + ct)$$

for $x' > x$ we get a similar term: $\frac{1}{2}\, g(x - ct)$, hence

10) $$\sigma\,(x,t) = \frac{1}{2}[g(x + ct) + g(x - ct)]$$

which is just D'Alembert's solution for infinite media. Q.E.D.

2. Proof that response to a general pulse is the same as Eq. (74).

In general,

$$11) \qquad \sigma(x,t) = \int_{t'} dt' \int_{x'} \frac{c}{2}\{H(\frac{|x - x'|}{c} - (t - t')] - 1\}f(t')g(x')$$

in our case

$$12) \qquad \sigma(x,t) = \frac{c}{2}\int_{t'} f(t')dt' \int_{0}^{x-c(t-t')} g(x')dx' + \int_{x+c(t-t')}^{\infty} g(x')dx' - \int_{0}^{\infty} g(x)'dx'$$

$$\sigma(x,t) = \frac{c}{2}\int f(t')dt' \int_{x+ct}^{x-ct} g(x')dx'$$

Now, integrate by parts

$$dU = f(t')dt'$$

$$13) \qquad U = \int f(t')dt' = F(t)$$

$$V = \int_{x+ct}^{x-ct} g(x')dx'$$

$$\frac{du}{dt'}\, dt' = -cg(x - ct) - c(g + ct)$$

since

$$\frac{d}{d\alpha}\int_{\phi_1(\alpha)}^{\phi_2(\alpha)} f(x,\alpha)dx = \int_{\phi_1}^{\phi_2} \frac{\partial f}{\partial \alpha}(x,\alpha)dx$$

$$- \phi_2'(\alpha)f(\phi_2(\alpha),\alpha) - \phi_1'f(\phi_1(\alpha),\alpha)$$

from hence

$$\sigma(x,t) = \frac{c}{2}\{\overbrace{\int f(t')dt'}^{F(t)} \int_{x+c\tau}^{x-c\tau} g(x')dx' \Big|_0^t$$

$$- c\int_{t'} - F(t')[g(x - c\tau) - g(x + c\tau)]dt'\}$$

$$\tau = t - t'$$

In the first term,

$$\text{when } t' = 0,\ F(t') = 0$$

16) $$\text{when } t' = t,\ \int_{x+c\tau}^{x-c\tau} g(x')dx' = \int_x^x g(x')dx = 0$$

thus,

17) $$\sigma(x,t) = \frac{c^2}{2}\int_{t'} F(t')[g(x - ct) + g(x + ct)]dt'$$

The original wave equation was

18) $$\frac{\partial^2\sigma}{\partial x^2} - \frac{1}{c^2}\frac{\partial^2\sigma}{\partial t^2} = \frac{\frac{\alpha E}{1 - 2\nu}}{c^2}\frac{\partial^2 T}{\partial t^2}$$

so the complete solution is

19) $$\sigma^0(x,t) = \int F(t')dt' \frac{1}{2}\left[\frac{\alpha E}{1 - 2\eta}\right][g(x - c\tau) + g(x + c\tau)]$$

if $x - ct > 0$; $\tau = t - t'$

this solution is valid for infinite media, so we must now account for the stress free boundary.

This can by the method of images in which a symmetric pulse is started at an image point as:

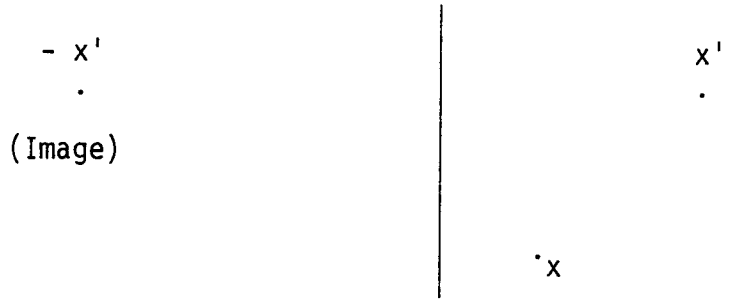

The effect is to add to the above solution a similar pulse and integrate over the appropriate Green's function:

20) $$\sigma' = \int_{t'} f(t')dt' \int_{x'} \frac{c}{2}\left[H\left(\frac{|x - (-x')|}{c} - (t - t') - 1\right](-g(x'))\right.$$

21) $$\sigma' = \int f(t')dt' \frac{c}{2}\left[\int_{c\tau - x}^{-\infty} g(x')dx' - \int_{0^-}^{-\infty} -g(x')dx'\right.$$

22) $$\sigma' = \int f(t')dt' \frac{c}{2}\int_{c\tau - x}^{0^-} g(x')dx'$$

as before

23) $$\sigma' = \frac{c}{2} F(t') \int_{c\tau - x}^{0^-} g(x')dx' \Big|_0^t$$

$$-c \int_{t'} - F(t')[g(0^-) + g(c\tau - x)]dt'$$

if $x - ct < 0$, since

24) $$g(0^-) = 0$$

$$F(0) = 0$$

$$g(-x) = 0$$

therefore,

$$\sigma' = -\frac{c^2}{2} \int F(t')g(c\tau - x)dt' \quad \text{if } x - ct < 0$$

adding equation (19) and (25) since

$$\sigma = \sigma^0 + \sigma'$$

$$\sigma(x,t) = \frac{\alpha E}{1 - 2\nu} \frac{1}{2} \int F(t')dt'[g(x + c\tau) + H(x - c\tau)g(x - c\tau) - H(c\tau - x)g(c\tau - x)]$$

$$\gamma = \frac{\alpha E}{1 - 2\nu} \qquad \tau = t - t'$$

which is identical with Eq. (74) upon substituting Eq. (72).

Q. E. D.

Reference for Appendix A

1. Methods of Theoretical Physics; Morse, P. M., and Feshback, H.; McGraw-Hill, 1953, p. 843.